*Economic Geology*, v. 115, no. 7, pp. 1519–1536

# Triple Oxygen ($\delta^{18}O$, $\Delta^{17}O$), Hydrogen ($\delta^{2}H$), and Iron ($\delta^{56}Fe$) Stable Isotope Signatures Indicate a Silicate Magma Source and Magmatic-Hydrothermal Genesis for Magnetite Orebodies at El Laco, Chile

Tristan Childress,[1,†] Adam C. Simon,[1] Martin Reich,[2,3] Fernando Barra,[2,3] Laura D. Bilenker,[4] Nikita L. La Cruz,[1] Ilya N. Bindeman,[5] and J. Tomás Ovalle[2,3]

[1]*Department of Earth and Environmental Sciences, University of Michigan, 1100 North University Ave., Ann Arbor, Michigan 48109-1005*

[2]*Department of Geology and Andean Geothermal Center of Excellence (CEGA), Universidad de Chile, Plaza Ercilla 803, Santiago, Chile*

[3]*Millennium Nucleus for Metal Tracing Along Subduction, Facultad de Ciencias Físicas y Matemáticas (FCFM), Universidad de Chile, Santiago, Chile*

[4]*Department of Geosciences, College of Sciences and Mathematics, Auburn University, 2050 Beard Eaves Memorial Coliseum, Auburn, Alabama 36849*

[5]*Department of Geological Sciences, University of Oregon, 1275 E 13th Ave., Eugene, Oregon*

## Abstract

The Plio-Pleistocene El Laco iron oxide-apatite (IOA) orebodies in northern Chile are some of the most enigmatic mineral deposits on Earth, interpreted to have formed as lava flows or by hydrothermal replacement, two radically different processes. Field observations provide some support for both processes, but ultimately fail to explain all observations. Previously proposed genetic models based on observations and study of outcrop samples include (1) magnetite crystallization from an erupting immiscible Fe- and P-rich (Si-poor) melt and (2) metasomatic replacement of andesitic lava flows by a hypogene hydrothermal fluid. A more recent investigation of outcrop and drill core samples at El Laco generated data that were used to develop a new genetic model that invokes shallow emplacement and surface venting of a magnetite-bearing magmatic-hydrothermal fluid suspension. This fluid, with rheological properties similar to basaltic lava, would have been mobilized by decompression-induced collapse of the volcanic edifice. In this study, we report oxygen, including $^{17}O$, hydrogen, and iron stable isotope ratios in magnetite and bulk iron oxide (magnetite with minor secondary hematite and minor goethite) from five of seven orebodies around the El Laco volcano, excluding San Vicente Bajo and the minor Laquito deposits. Calculated values of $\delta^{18}O$, $\Delta^{17}O$, $\delta D$, and $\delta^{56}Fe$ fingerprint the source of the ore-forming fluid(s): $\Delta^{17}O_{sample} = \delta^{17}O_{sample} - \delta^{18}O_{sample} * 0.5305$. Magnetite and bulk iron oxide (magnetite variably altered to goethite and hematite) from Laco Sur, Cristales Grandes, and San Vicente Alto yield $\delta^{18}O$ values that range from 4.3 to 4.5‰ ($n = 5$), 3.0 to 3.9‰ ($n = 5$), and –8.5 to –0.5‰ ($n = 5$), respectively. Magnetite samples from Rodados Negros are the least altered samples and were also analyzed for $^{17}O$ as well as conventional $^{16}O$ and $^{18}O$, yielding calculated $\delta^{18}O$ values that range from 2.6 to 3.8‰ ($n = 9$) and $\Delta^{17}O$ values that range from –0.13 to –0.07‰ ($n = 5$). Bulk iron oxide from Laco Norte yielded $\delta^{18}O$ values that range from –10.2 to +4.5‰ (avg = 0.8‰, $n = 18$). The $\delta^{2}H$ values of magnetite and bulk iron oxide from all five orebodies range from –192.8 to –79.9‰ ($n = 28$); hydrogen is present in fluid inclusions in magnetite and iron oxide, and in minor goethite. Values of $\delta^{56}Fe$ for magnetite and bulk iron oxide from all five orebodies range from 0.04 to 0.70‰ (avg = 0.29‰, $\sigma = 0.15$‰, $n = 26$). The iron and oxygen isotope data are consistent with a silicate magma source for iron and oxygen in magnetite from all sampled El Laco orebodies. Oxygen ($\delta^{18}O$ $\Delta$ +4.4 to –10.2‰) and hydrogen ($\delta^{2}H \simeq$ –79.9 to –192.8‰) stable isotope data for bulk iron oxide samples that contain minor goethite from Laco Norte and San Vicente Alto reveal that magnetite has been variably altered to meteoric values, consistent with goethite in equilibrium with local $\delta^{18}O$ and $\delta^{2}H$ meteoric values of $\simeq$ –15.4 and –211‰, respectively. The $H_2O$ contents of iron oxide samples from Laco Norte and San Vicente Alto systematically increase with increasing abundance of goethite and decreasing values of $\delta^{18}O$ and $\delta^{2}H$. The values of $\delta^{2}H$ ($\simeq$ –88 to –140‰) and $\delta^{18}O$ (3.0–4.5‰) for magnetite samples from Cristales Grandes, Laco Sur, and Rodados Negros are consistent with growth of magnetite from a degassing silicate melt and/or a boiling magmatic-hydrothermal fluid; the latter is also consistent with $\delta^{18}O$ values for quartz, and salinities and homogenization temperatures for fluid inclusions trapped in apatite and clinopyroxene coeval with magnetite. The sum of the data unequivocally fingerprint a silicate magma as the source of the ore fluids responsible for mineralization at El Laco and are consistent with a model that explains mineralization as the synergistic result of common magmatic and magmatic-hydrothermal processes during the evolution of a caldera-related explosive volcanic system.

## Introduction

Investigations to determine the genesis of iron oxide-apatite (IOA) deposits have been ongoing for decades, with proposed models that range from those that invoke purely hydrothermal processes to those invoking purely magmatic processes. One of the most enigmatic and hotly debated deposits is the El Laco IOA deposit, located at about 5,000 masl in the Chilean Altiplano (Fig. 1). Park (1961) documented the outcrops at El Laco and hypothesized the orebodies represent surficial

†Corresponding author: e-mail, tristanc@umich.edu

 *Submitted: April 24, 2019 / Accepted: February 26, 2020*

or shallow intrusion of iron oxide lava flows, citing textures among the iron oxide orebodies that resemble aa, pahoehoe, volcanic bombs, and vesicular bubble-like shapes. At El Laco, two opposing models have been proposed and tested at length to explain the coexistence of arguably volcanic and hydrothermal features of the orebodies: liquid immiscibility (Naslund et al., 2002; Tornos et al., 2016, 2017; Velasco et al., 2016; Xie et al., 2019) and hydrothermal replacement of andesitic lava flows (Rhodes and Oreskes, 1995; Rhodes et al., 1999; Sillitoe and Burrows, 2002; Dare et al., 2015).

The liquid immiscibility hypothesis, originally proposed by Philpotts (1967) to explain the magmatic/volcanic textures observed in many IOA deposits, invokes unmixing of a silicate melt into two physicochemically distinct melts, one Fe- and P-rich and the other Si-rich and Fe-poor (Naslund et al., 2002). In order for the Fe-P-rich melt to ascend from its source magma into the overlying crust and form an orebody, the model requires that $H_2O$ partition preferentially into the Fe-P-rich melt in order to lower its density and increase its buoyancy relative to the conjugate Si-rich melt (Tornos et al., 2016, 2017). In contrast, the replacement model calls upon a hypogene Fe-rich hydrothermal fluid to percolate through andesitic lava flows and entirely replace the host rock with magnetite and hematite and, importantly, preserve all original volcanic textures (Rhodes et al., 1999; Sillitoe and Burrows, 2002; Dare et al., 2015). A new model to explain the formation of the El Laco orebodies was proposed by Ovalle et al. (2018) based on extensive textural and geochemical evidence for magnetite from surface and drill core samples. Those authors proposed that the El Laco orebodies formed by eruption of a buoyant magnetite-fluid suspension that evolved from a silicate magma. Their model is based on Knipping et al. (2015a, b), who invoked crystallization of magnetite microlites from an intermediate silicate melt, followed by volatile saturation of the melt wherein the surface of magnetite microlites are preferentially wetted and swept up by the volatile phase to form a magnetite-fluid suspension (i.e., mineral froth) that has a lower density than the surrounding melt.

In this study, we measure Fe, O, and H stable isotope compositions of magnetite, hematite, and goethite samples from five of the six largest deposits at El Laco to identify the source of the ore-forming fluids and use the data to assess these three competing genetic hypotheses. In addition to conventional oxygen stable isotopes (i.e., $\delta^{18}O$), we report the first $\Delta^{17}O$ values of iron oxides from an IOA deposit and demonstrate that the combined use of conventional (i.e., $\delta^{18}O$) and non-

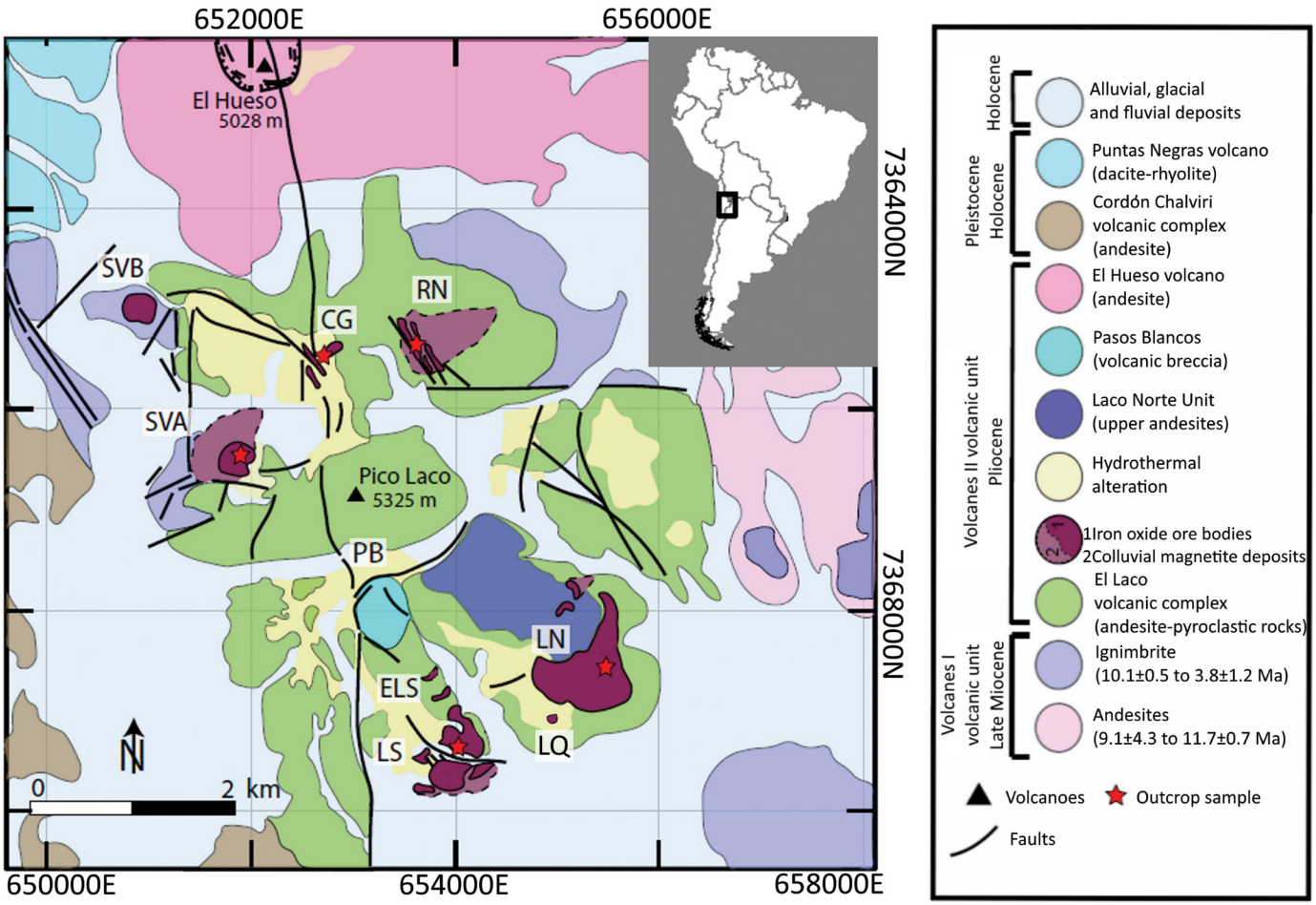


Fig. 1. Geologic map of El Laco from Ovalle et al. (2018). The El Laco Volcanic Complex is primarily composed of andesite and pyroclastic rocks (green) with major iron oxide deposits (maroon). Red stars denote sampling locations. CG = Cristales Grandes, ELS = Extensión Laco Sur, LN = Laco Norte, LS = Laco Sur, LQ = Laquito, RN = Rodados Negros, SVA = San Vicente Alto, SVB = San Vicente Bajo.

conventional ($\delta^{56}$Fe, $\Delta^{17}$O) stable isotopes fingerprint the source reservoir(s) for ore fluids and provide new insights into the formation of IOA systems.

## Geologic Background

The El Laco Volcanic Complex is located in a structurally controlled volcanic zone of the Central Andes (23°48′ S, 67°30′ W; Fig. 1) and records an uncommon set of both magmatic and hydrothermal stages. It is composed of variably preserved andesitic to dacitic lava flows, pyroclastic rocks, and volcanic breccias, which are the products of several stages of volcanic activity developed from the Pliocene to the Pleistocene (5.3 ± 1.9–1.6 ± 0.5 Ma; K-Ar; Naranjo et al., 2010). These volcanic products host large iron oxide orebodies with remarkably volcanic and subvolcanic features, which have been dated to 2.1 ± 0.1 Ma (apatite fission track, Maksaev et al., 1988). In addition, extensive zones of penetrative hydrothermal alteration are widespread among the andesites at El Laco (Rhodes and Oreskes, 1995, 1999; Rhodes et al., 1999).

Stratigraphically, from oldest to youngest, the major volcanic units are described as the lower andesites, upper andesites, dome-like edifices, and volcanic breccia bodies that crosscut the older units. The majority (>90%) of the andesitic volcanic materials are porphyritic, massive, rarely vesicular, and contain abundant plagioclase and pyroxene phenocrysts. Unaltered andesites are silica oversaturated according to the total alkali-silica (TAS) classification diagram (Le Maitre et al., 2005), where they plot near the silica-saturated trachyandesite field and are geochemically similar to nearby recent edifices such as Llullaillaco and Lascar (Matthews et al., 1999; Velasco et al., 2016). The El Laco andesites are calc-alkaline I-type rocks that range in composition from basaltic andesite to primitive dacite, and their chemistry does not vary significantly among magmatic pulses (Velasco et al., 2016).

The magnetite orebodies are located around the central volcanic plug (Pico Laco), structurally associated with collapse-related fissures and secondary craters (Frutos and Oyarzun, 1975; Naranjo et al., 2010; Ovalle et al., 2018). Based on their morphologies and surface textures, they can be classified as stratabound (Laco Norte, Laco Sur, Laquito, San Vicente Alto), dome-shaped (San Vicente Bajo), and tabular (Rodados Negros, Cristales Grandes). A recent study by Ovalle et al. (2018) reported that such orebodies show a complex vertical zonation, comprising an outcropping portion of trace element-depleted massive magnetite (e.g., Ti: 218 ppm and V: 586 ppm, average contents), which is partially to totally martitized (oxidized), and contains minor clinopyroxene, apatite, and REE and iron phosphates. Upper massive magnetite grades at depth to large magnetite-(±clinopyroxene-scapolite) breccia bodies, characterized by a systematic increase of Ti in magnetite with depth (average contents of up to 7637 ppm; Ovalle et al., 2018). Magnetite from surface (focus of this study) exhibits a variety of textures. Massive stratabound orebodies (listed above) are dominated by flow and highly vesicular textures, as well as octahedral and pyroclastic-like or friable magnetite. Whereas tabular orebodies (listed above) are characterized by subvolcanic cooling textures, such as columnar and bladed magnetite, and generally lack vesicularity (Figs. 2, 3). Highly vesicular, friable magnetite is found in abundance at Laco Sur and occurs elsewhere to lesser degrees (Nyström et al., 2016). Columnar magnetite is observed locally within the deposits, and numerous vertically oriented gas escape tubes lined with octahedral magnetite are found at Laco Sur, Laco Norte, and San Vicente Alto; the tubes themselves range up to tens of centimeters in diameter and up to meters in height. Hydrothermal alteration at El Laco occurs widespread both on surface and at depth, and although it appears to be spatially close to the iron bodies, there is not always a synchronous relationship between hydrothermal alteration and iron oxide mineralization (Tornos et al., 2017). Aureoles that are pervasive in the andesite surrounding the magnetite bodies consist of a magnetite-diopside-quartz assemblage (Vivallo et al., 1994; Rhodes et al., 1999). At depth, an alkali-calcic alteration assemblage is particularly well developed and comprises intense scapolitization and diopside formation that partially to pervasively replace andesitic fragments, which occur immersed in a magnetite-diopside-scapolite matrix (Rhodes et al., 1999; Naranjo et al., 2010; Ovalle et al., 2018). Late magnetite-clinopyroxene-pyrite and pyrite-bearing gypsum veinlets crosscut the breccia body at depth (Ovalle et al., 2018). Andesite is locally crosscut by coarse-grained veins with unidirectional growth mainly composed of diopside, magnetite, and anhydrite (Tornos et al., 2016). Weak regional propylitic alteration (chlorite-epidote-sericite; Vivallo et al., 1994; Rhodes et al., 1997) appears to temporally overlap sodic, potassic, and calcic alteration (Rhodes et al., 1999). Widespread andesite bleaching at El Laco is a result of a late argillic alteration, which occurs as extensive steam-heated zones marked by a penetrative replacement of andesites by argillic assemblages dominated by tridymite, cristobalite, alunite, jarosite, trace secondary copper minerals, and minor native sulfur, forming silicic vein-like structures and irregular hydrothermal breccia bodies (Vivallo et al., 1994; Sillitoe and Burrows, 2002). In addition, large exhalative deposits represented by gypsum-rich mounds, which appear to be fossil fumaroles, are located in discrete emission centers spatially associated with NW-trending collapse structures, which control the late hot-spring-like geothermal activity at El Laco Volcanic Complex (Rhodes and Oreskes, 1995; Vivallo et al., 1994). Sulfate-rich alteration altered magnetite to hematite in some orebodies and replaced andesite with alunite and minor kaolinite, gypsum, and tridymite, and gypsum veins locally crosscut magnetite in several deposits (Sillitoe and Burrows, 2002).

## Methods

### *Sample selection*

Access to El Laco was provided by CAP Minería. Samples were collected from five of the seven surficial iron oxide deposits: Laco Norte, Laco Sur, Rodados Negros, Cristales Grandes, and San Vicente Alto. San Vicente Bajo, and Laquito were not sampled due to poor road conditions that prohibited access during field work. Sites range in elevation from about 4,640 masl at Laco Sur to >5,000 masl at Cristales Grandes. Samples at each site were selected in the field for their uniqueness in texture and appearance (e.g., columnar magnetite, octahedral magnetite, volcanic bomb-like) in order to sample a wide variety of textural types. With the exception of samples from

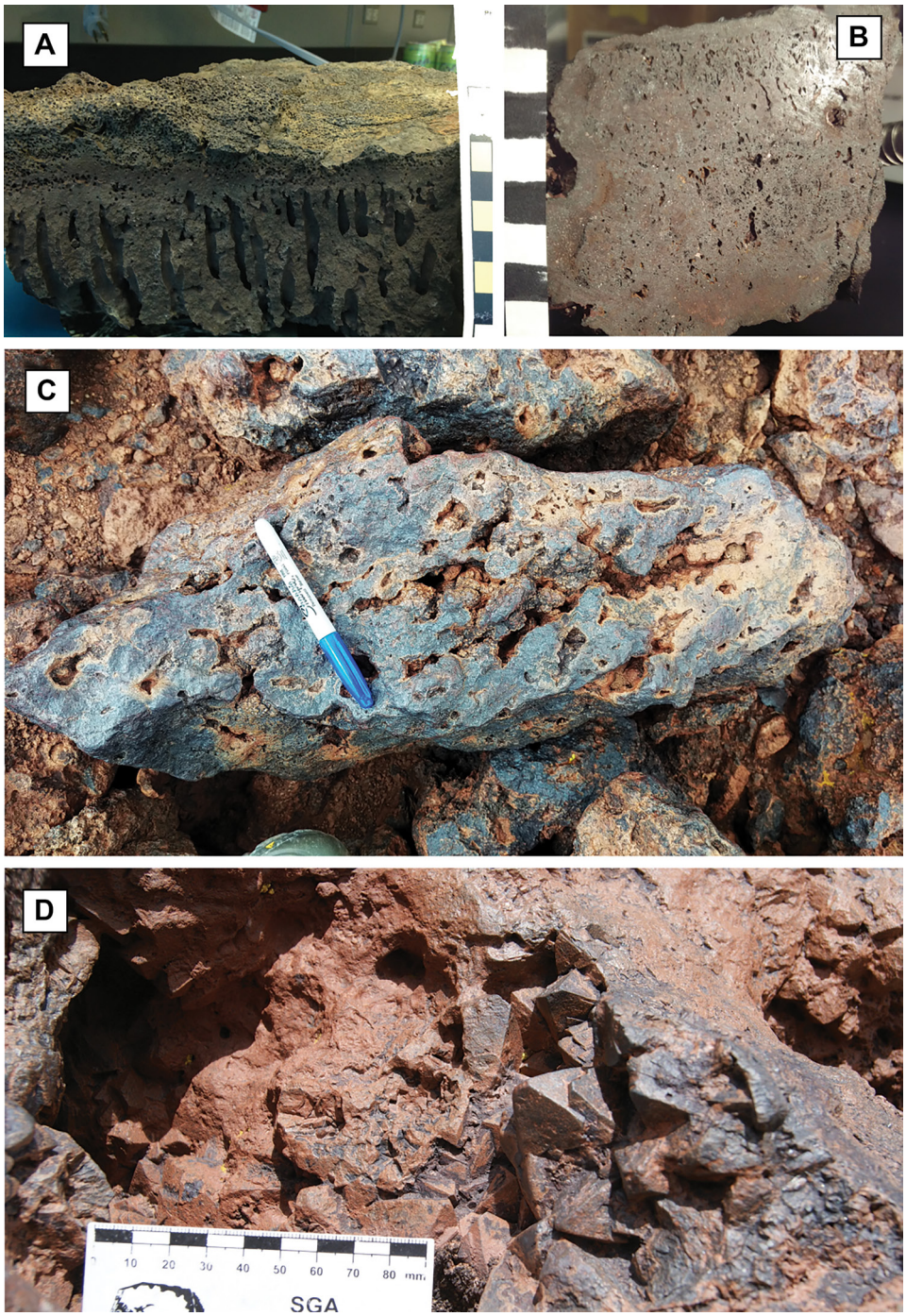


Fig. 2. A. Vesicular basalt sample from Hawaii. B. and C. Vesicular magnetite from Laco Norte and Rodados Negros, respectively. Vesicular textures are nearly ubiquitous among the iron oxide deposits at El Laco, along with bomb textures, demonstrating the volatile rich and fast cooling nature of these samples. Terminal euhedral magnetite tends to line the inner walls of vesicles. Scales in (A) and (B) are in centimeters; marker for scale in (C).

Cristales Grandes and San Vicente Alto that contain large apatite and diopside crystals, iron oxide hand samples were free of visible noniron oxides.

*Sample preparation for stable isotope analysis*

Sample preparation followed the same procedures described in Bilenker et al. (2016, 2017) and Childress et al. (2016, 2020). Samples of iron oxide were cut by diamond saw into small cubes in order to exclude, as much as possible, all nonmagnetic minerals. Samples were then wrapped in weighing paper and crushed with a plastic-sheathed mallet to reduce the grain size to less than 1 mm and disaggregate iron oxides and any gangue minerals. Magnetite grains were then separated from the crushed material by use of a hand magnet wrapped in a

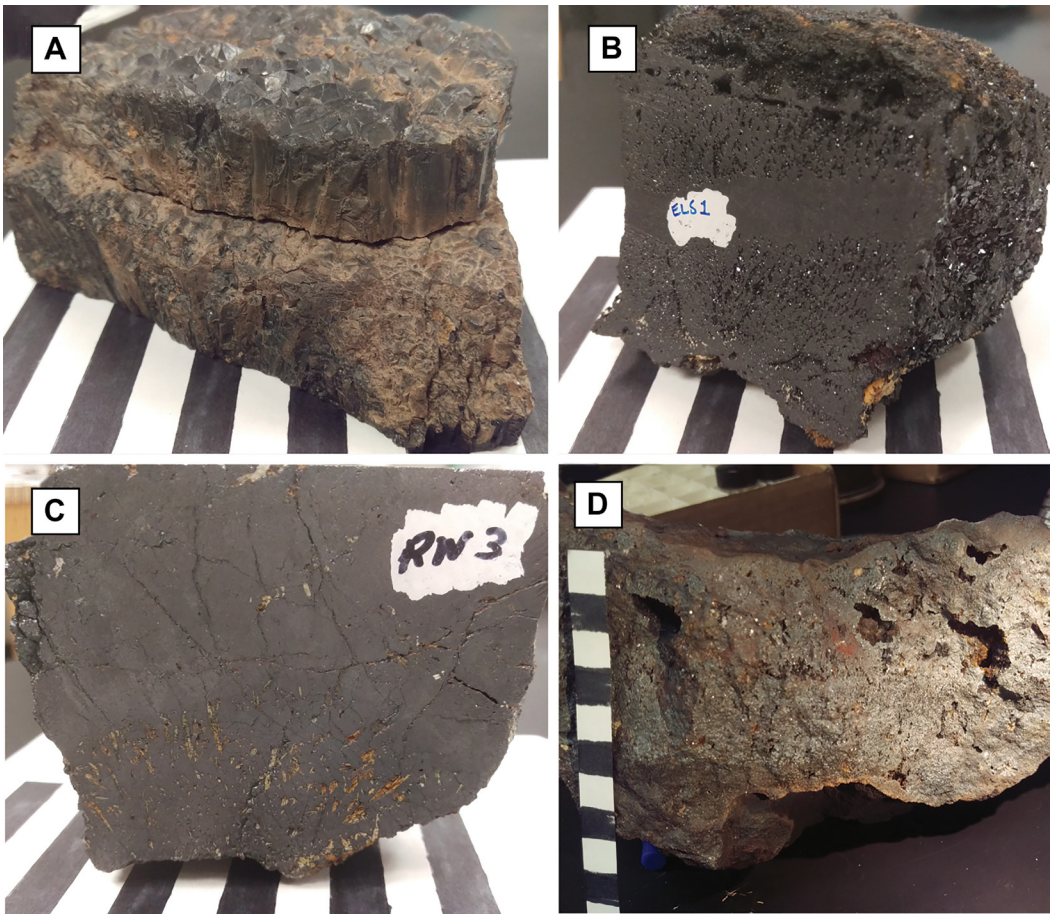


Fig. 3. Select hand samples from El Laco. A. and C. Hand samples RN-4 and RN-3, respectively, featuring columnar magnetite from Rodados Negros with octahedral terminations and oriented diopside in (C). B. Highly vesicular magnetite from Laco Sur (LS-1). D. Highly vesicular and oxidized magnetite from San Vicente Alto, similar to samples analyzed in this study. Black and white scale bars are 1 cm wide.

Kimwipe. The separated iron oxides grains were inspected by using a binocular microscope at ~40× magnification and only the most uniform grains were handpicked. Grain sizes of magnetite between ~0.1 and 0.8 mm were selected for hydrogen, iron and oxygen isotope analyses. These grains were visually estimated to contain ≥95% magnetite for samples from Laco Sur, Cristales Grandes, and Rodados Negros. Samples from Laco Norte and San Vicente Alto were visually estimated to contain <95% magnetite and in some cases were primarily hematite and goethite and are referred to as bulk iron oxide samples. Figure 4 shows typical iron oxide textures in these samples, including magnetite replaced by hematite with goethite filling space between grains at Laco Norte (panel 4A), relatively homogeneous magnetite from Rodados Negros and Cristales Grandes (panels 4B and 4C), and magnetite intergrown with occasional $FePO_4$ replacing apatite at San Vicente Alto (panel 4D). Approximately 10, 2 to 3, and 0.5 to 1.5 mg of sample were used for hydrogen, oxygen and iron isotope analyses, respectively.

Grains selected for iron isotope analysis were further crushed to hasten acid digestion by use of an alumina ceramic mortar and pestle that were cleaned with ethanol and compressed air between samples to avoid contamination. Aliquots of polished magnetite and bulk iron oxide grains from all samples were inspected at high magnification using backscattered-electron (BSE) imaging on a Cameca SX-100 electron probe microanalyzer (EPMA) and separately on a JEOL-7800FLV field emission-scanning electron microscope (FE-SEM); both instruments are located at the University of Michigan Electron Microbeam Analysis Lab (EMAL). Magnetite and bulk iron oxides from the samples analyzed in the current study were also analyzed via EPMA (Ovalle et al., 2018) and LA-ICP-MS (La Cruz et al., 2020) to determine their major, minor, and trace element contents.

### *Oxygen isotopes*

Oxygen isotope analyses of iron oxides were conducted at the University of Oregon using a laser fluorination line coupled with a Thermo-Finnigan MAT 253 gas isotope ratio mass spectrometer (IRMS) in dual inlet mode. Iron oxide grains (2–3 mg) from each sample were subjected initially to low-power lasing. Laser power was slowly increased to minimize jumping movements of the grains during fluorination with $BrF_5$. For samples that did not experience grain jumping, $O_2$ yields were close to the theoretical 100%. All data were compared to the Gore Mountain garnet (in-house standard, UOG,

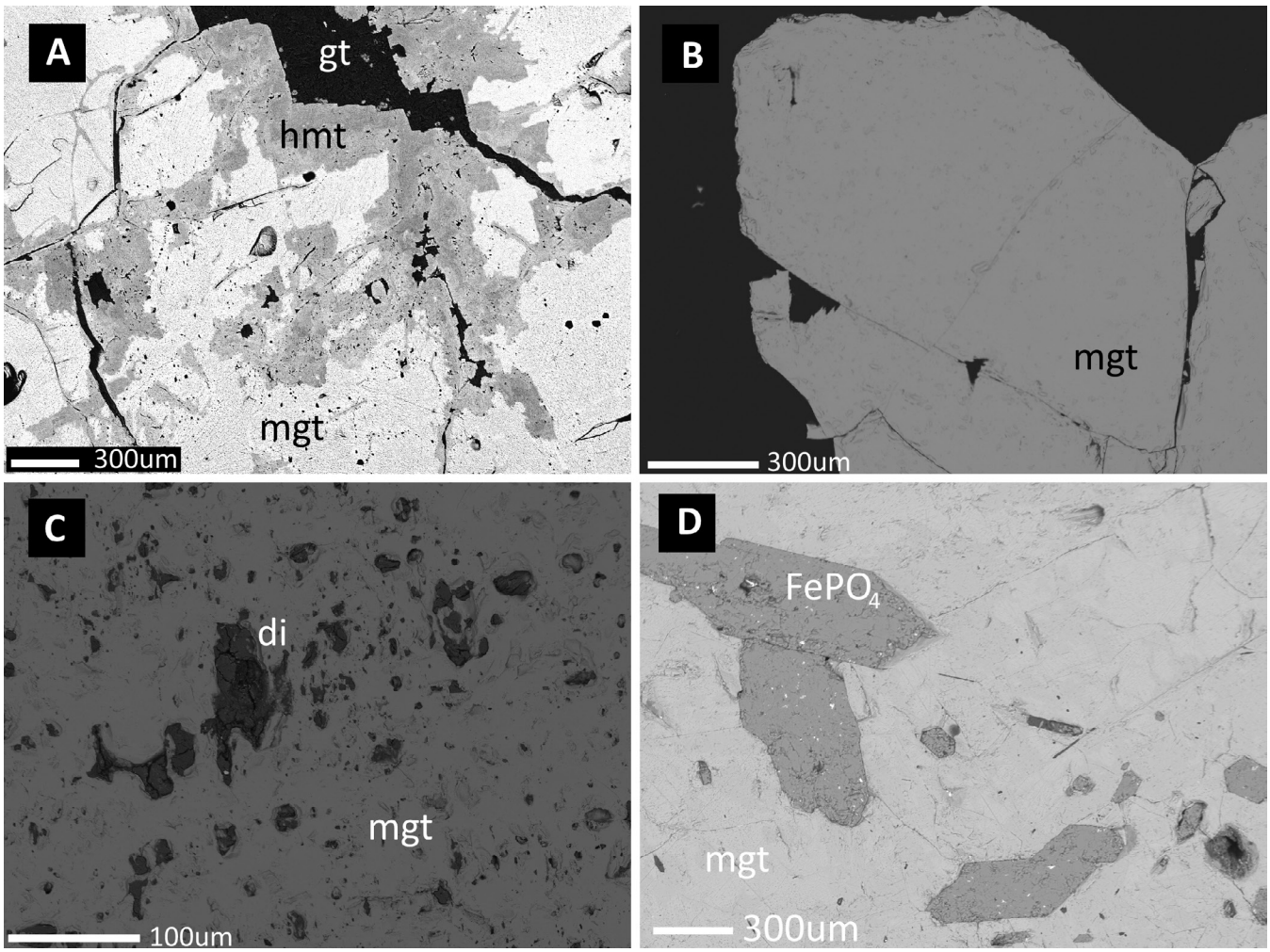


Fig. 4. Backscattered electron images of typical magnetite textures from El Laco. A. Magnetite (mgt) being replaced by hematite (hmt) on outer rims, with goethite (gt) filling space between grains (LN-2). B. Homogeneous magnetite from Rodados Negros (RN-1; black area is epoxy). C. Magnetite intergrown with diopside (di) at Cristales Grandes (CG-5). D. Magnetite intergrown with $FePO_4$ that has replaced apatite (SVA-1).

recommended 6.52‰), which was measured before, during, and after analysis of iron oxide samples to correct for instrumental drift. The average value for standard UOG ($\delta^{18}O_{UOG}$) was 6.50‰ and the average $2\sigma$ for UOG for each day of analysis was ~0.27‰ ($n$ = 14), calculated from variance. Individual sample analyses typically have $2\sigma$ of <0.1‰. Theoretical $O_2$ yields for magnetite, hematite, and goethite are 8.64, 9.39, and 11.25 μmol/mg, respectively. Oxygen isotope values are reported relative to the international Vienna Standard Mean Ocean Water (VSMOW) and were calculated using equation (1):

$$\delta^{18}O_{sample}\ (‰) = [(^{18}O/^{16}O)_{measured}/(^{18}O/^{16}O)_{VSMOW} - 1] \cdot 1{,}000. \quad (1)$$

The average $\delta^{18}O$ and $\Delta^{17}O$ of UOG during $\Delta^{17}O$ analyses were 6.41 ± 0.01‰ and -0.12 ± 0.01‰ ($2\sigma$, n = 3), respectively. Capital delta values were calculated using equation (2):

$$\Delta^{17}O_{sample} = \delta^{17}O_{sample} - \delta^{18}O_{sample} \cdot 0.5305, \quad (2)$$

where 0.5305 is the slope of the reference line for minerals formed at high temperatures (Pack et al., 2016). Five samples from Rodados Negros were analyzed three times and averaged.

Triple oxygen isotopes were measured in a single session with $O_2$ gas as analyte run against calibrated reference gas, and an additional gas chromatographic purification step in a controlled helium flow using a 6-ft-long zeolite column that was added to the University of Oregon fluorination line (Bindeman et al., 2018). This procedure is needed to minimize potential $^{17}O$ contaminants (Pack et al., 2016), such as NF and organics. The error in $\delta^{18}O$ measurements is ±0.2‰ 1SE when $\Delta^{17}O$ is also measured; the $\Delta^{17}O$ error is ±0.01‰ 1SE.

### *Hydrogen isotopes*

Hydrogen isotope analyses of iron oxides were also conducted at the University of Oregon by using a Thermo Scientific high-temperature conversion elemental analyzer (TC/EA) with a MAT253 gas source IRMS, following the procedure described in Bindeman et al. (2012). We used a glassy carbon reactor held at 1,450°C and gas chromatographic peak separation, using continuous He flow and a CONFLOW gas interface. The

reference materials USGS57 (biotite) and USGS58 (muscovite) (Qi et al., 2017) were measured throughout the analytical session to account for a range of $\delta^2$H values, and were measured to be –91.0‰ ($n$ = 5, 2$\sigma$ = 9.7‰) and –28.0‰ ($n$ = 5, 2$\sigma$ = 4.7‰), respectively, with calculated wt % $H_2O$ contents of 3.60 ($n$ = 5, 2$\sigma$ = 0.11%) and 4.11 ($n$ = 5, 2$\sigma$ = 0.04%), respectively. Water was determined by peak integration of H and D areas relative to that of the known NBS30 and USGS57 micas (nominal $H_2O$ = 3.5 wt %). Samples with measured $H_2O$ contents <0.05 wt % were not used in this study. Results are reported relative to VSMOW, calculated using equation (3):

$$\delta^2H_{sample}\ (‰) = [(^2H/^1H)_{measured}/(^2H/^1H)_{VSMOW} - 1] \cdot 1{,}000. \quad (3)$$

*Iron isotopes*

Iron oxide samples were subjected to ion exchange chromatography to isolate Fe for isotopic analysis. Between ~0.5 and 1.5 mg of each sample was dissolved in aqua regia and dried down, dissolved again in 8*N* HCl, and then loaded into columns of AG1-X8 resin (Biorad, 200–400 mesh) in 8*N* HCl, following the procedure described by Huang et al. (2011). Analyses were performed at the Pacific Centre for Isotopic and Geochemical Research, University of British Columbia, Canada, using a Nu Plasma 1700 multicollector-inductively coupled plasma-mass spectrometer (MC-ICP-MS) in dry plasma mode with a DSN-100. The large geometry of the instrument allowed for complete separation of Ar interferences in high resolution. Cr was monitored and $^{54}$Fe and measurements were corrected because of isobaric interference with $^{54}$Cr. Each sample was analyzed three to four times, with all analyses bracketed by the international standard IRMM-14 to correct for small changes in mass bias over time. Average IRMM-14 measured 0.00‰, (2$\sigma$ = 0.077, $n$ = 12; Millet et al., 2012). Iron isotope values (Table 1) are reported relative to IRMM-14, calculated by using equation (4):

$$\delta^{56}Fe_{sample}\ (‰) = [(^{56}Fe/^{54}Fe)_{measured}/(^{56}Fe/^{54}Fe)_{IRMM\text{-}14} - 1] \cdot 1{,}000. \quad (4)$$

## Results

*Oxygen isotope compositions*

Stable oxygen isotope ratios for magnetite and bulk iron oxide are reported as $\delta^{18}$O and $\Delta^{17}$O in Tables 1 and 2, respectively. The $\delta^{18}$O values (±2$\sigma$) range from very low meteoric –10.15‰ to normal magmatic +4.49‰. All negative values occur in samples from either Laco Norte or San Vicente Alto and correspond to a decrease in magnetite abundance and increase in (secondary) hematite and/or goethite, demonstrated by significant increase in analytical $O_2$ yields. The $\delta^{18}$O values (±2$\sigma$) for individual deposits Laco Norte, Laco Sur, Rodados Negros, Cristales Grandes, and San Vicente Alto average 0.81 ± 9.07 ($n$ = 18), 4.41 ± 0.14 ($n$ = 5), 3.69 ± 0.21 ($n$ = 9), 3.65 ± 0.71 ($n$ = 5), and –3.77 ± 8.39‰ ($n$ = 5), respectively. Five samples from Rodados Negros were analyzed for $^{16}$O, $^{17}$O, and $^{18}$O, with those data used to calculate $\Delta^{17}$O, yielding $\Delta^{17}$O values of –0.13, –0.12, -0.09, –0.07, and –0.07‰. Each sample was analyzed three times for $^{16}$O, $^{17}$O, and $^{18}$O, and all samples have $\Delta^{17}$O 2$\sigma$ ≤0.02 except RN2 which is 0.04.

*Hydrogen isotope compositions*

Stable hydrogen isotope ratios for magnetite and bulk iron oxide are reported as $\delta^2$H in Table 1. The $\delta^2$H values (±2$\sigma$) range from –192.8 to –79.9‰ and average –133.0 ± 56.2‰. The average $\delta^2$H values (±2$\sigma$) for individual deposits Laco Norte, Laco Sur, Rodados Negros, Cristales Grandes, and San Vicente Alto are –150.9 ± 68.1 ($n$ = 11), –121.4 ± 13.1 ($n$ = 5), –100.0 ± 24.7 ($n$ = 4), –129.8 ± 23.9 ($n$ = 3), and –133.8 ± 14.8‰ ($n$ = 5), respectively. Calculated $H_2O$ contents ($H_2O_{equiv}$) for Laco Norte, Laco Sur, Rodados Negros, Cristales Grandes, and San Vicente Alto average (±2$\sigma$) 0.68 ± 1.23 ($n$ = 11), 0.13 ± 0.11 ($n$ = 5), 0.10 ± 0.08 ($n$ = 4), 0.14 ± 0.18 ($n$ = 3), and 1.06 ± 0.90 wt % ($n$ = 5), respectively, and may originate from either fluid inclusions, H within goethite, or both.

*Fe isotope compositions*

Stable iron isotope ratios for magnetite and bulk iron oxides are reported as $\delta^{56}$Fe in Table 1. Reference material UB-N was analyzed alongside the samples and yielded a $\delta^{56}$Fe value of 0.06 ± 0.1‰ ($n$ = 4), which is in good agreement with previous studies (e.g., Craddock and Dauphas, 2011). The $\delta^{56}$Fe values (±2$\sigma$) range from 0.04 ± 0.06 to 0.7 ± 0.03‰ and average 0.29 ± 0.15‰ ($n$ = 26). The $\delta^{56}$Fe values (±2$\sigma$) for individual deposits Laco Norte, Laco Sur, Rodados Negros, Cristales Grandes, and San Vicente Alto average 0.27 ± 0.13 ($n$ = 6), 0.35 ± 0.09 ($n$ = 5), 0.17 ± 0.02 ($n$ = 5), 0.20 ± 0.11 ($n$ = 5), and 0.47 ± 0.15‰ ($n$ = 5), respectively.

## Discussion

*Magmatic and magmatic-hydrothermal $\delta^{18}$O and $\Delta^{17}$O*

One of the major issues dividing opinion on the origin of the El Laco orebodies is the observation of textures on an outcrop scale that are interpreted to be the result of hydrothermal or magmatic processes. Rhodes and Oreskes (1999) carried out the first comprehensive stable isotope study of samples from El Laco with the goal to determine whether or not the magnetite-rich orebodies formed by a combination of magmatic and hydrothermal metasomatic processes or only by hydrothermal metasomatism of andesitic lava flows. Those authors hypothesized that if magnetite in the orebodies formed by crystallization from silicate melt and by precipitation from hydrothermal fluid, there should be two populations of $\delta^{18}$O values among the primary magnetite samples that exhibit textures interpreted to be magmatic and samples that are interpreted to exhibit hydrothermal textures. Rhodes and Oreskes (1999) reported $\delta^{18}$O values for magnetite and bulk iron oxide (i.e., magnetite variably altered to hematite) from surface samples from the same five orebodies as the current study, as well as samples from San Vicente Bajo and Laquito, and also whole-rock samples of altered and unaltered andesite host rock from El Laco. Their analyses of unaltered samples of both textural types of magnetite revealed a very narrow range of $\delta^{18}$O values (i.e., mean ±2$\sigma$ for all samples = 4.1 ± 0.49‰, total range = 1.7‰, $n$ = 16), where unaltered is defined as magnetite samples with ≤6 % hematite. Their data indicate that the $\delta^{18}$O values of magmatic- and hydrothermal-textured magnetite statistically overlap. Those authors reported that the $\delta^{18}$O values for hematite-bearing iron oxide samples become progressively lighter with increasing hematite content, which they interpreted to

Table 1. List of Samples Analyzed from El Laco for O, H, and Fe Isotopes and Respective Measurements

| Sample | $\delta^{18}O$ (‰) | µmol/milligram | $\delta^{2}H$ (‰) | $H_2O$ (wt %) | $\delta^{56}Fe$ (‰) | $2\sigma$ |
|---|---|---|---|---|---|---|
| LN-2 | –10.2 | 9.4 | –192.8 | 2.23 | 0.31 | 0.03 |
| LN-3a | 3.9 | 8.3 | –126.8 | 0.37 | | |
| LN-3b | 4.4 | 7.4 | –116.9 | 0.05 | | |
| LN-5 | 3.7 | 8.6 | –134.9 | 0.43 | | |
| LN-6a | 4.1 | 7.3 | -79.9 | 0.06 | | |
| LN-6b | 4.5 | 8.7 | | | | |
| LN-7 | 2.3 | 8.5 | | | | |
| LN-8 | 1.7 | 8.5 | | | | |
| LN-9 | 1.1 | 9.3 | –152.4 | 0.61 | 0.43 | 0.08 |
| LN-10a | 2.4 | 8.5 | –156.4 | 0.76 | 0.24 | 0.09 |
| LN-10b | 3.9 | 8.8 | –181.1 | 0.52 | 0.33 | 0.04 |
| LN-11a | –1.2 | 8.2 | | | | |
| LN-11b | 4.2 | 6.9 | | | | |
| LN-12 | -4.1 | 9.0 | –166.3 | 0.37 | | |
| LN-14a | 2.1 | 8.3 | –162.7 | 0.93 | 0.26 | 0.06 |
| LN-14b | -4.3 | 8.9 | –189.4 | 1.18 | 0.04 | 0.06 |
| LN-15 | 4.1 | 7.7 | | | | |
| LN-B | –8.2 | 9.7 | | | | |
| LS-1 | 4.5 | 8.5 | –127.4 | 0.09 | 0.35 | 0.04 |
| LS-2a | 4.4 | 7.9 | –127.9 | 0.21 | 0.28 | 0.08 |
| LS-2b | 4.4 | 7.9 | | | 0.28 | 0.08 |
| LS-3 | 4.3 | 7.0 | –111.9 | 0.15 | 0.28 | 0.06 |
| LS-t2 | 4.4 | 7.6 | –120.2 | 0.08 | 0.34 | 0.06 |
| LS-t5 | 4.4 | 7.4 | –119.7 | 0.10 | 0.51 | 0.09 |
| SVA-1 | –1.0 | 8.5 | –131.4 | 0.56 | 0.50 | 0.03 |
| SVA-2 | –8.5 | 7.7 | –145.0 | 1.37 | 0.70 | 0.03 |
| SVA-3 | -0.6 | 9.4 | –128.8 | 1.32 | 0.44 | 0.07 |
| SVA-4 | -0.5 | 9.0 | –137.2 | 0.58 | 0.36 | 0.06 |
| SVA-t1 | –8.2 | 9.4 | –126.7 | 1.46 | 0.03 | 0.06 |
| CG-1 | 3.7 | 8.0 | | | 0.24 | 0.1 |
| CG-2 | 3.9 | 7.7 | | | 0.30 | 0.02 |
| CG-3 | 3.0 | 8.7 | –132.4 | 0.24 | 0.29 | 0.05 |
| CG-4 | 3.9 | 8.3 | –140.3 | 0.08 | 0.07 | 0.07 |
| CG-5 | 3.7 | 8.0 | –116.8 | 0.09 | 0.11 | 0.02 |
| RN-1 | 3.8 | 8.3 | –116.9 | 0.10 | 0.18 | 0.03 |
| RN-2 | 3.6* | - | -94.6 | 0.15 | 0.18 | 0.02 |
| RN-3 | 3.8 | 8.1 | –100.5 | 0.09 | 0.14 | 0.03 |
| RN-4 | 3.7 | 8.1 | | | 0.16 | 0.07 |
| RN-5 | 3.5 | 7.9 | –88.0 | 0.05 | 0.20 | 0.05 |

Notes: Theoretical yields of $O_2$ for magnetite, hematite, and goethite are 8.64, 9.39, and 11.25 µmol/milligram, respectively; blank spaces indicate samples that were not analyzed for Fe, O, or H; $\delta^{2}H$ and $\delta^{18}O$ values are reported relative to VSMOW; individual $\delta^{18}O$ typically have $2\sigma$ <0.1 ‰; $\delta^{56}Fe$ is reported relative to IRMM–14; *sample RN-2 value reported from $\Delta^{17}O$ analysis in Table 2

be the result of later stage interaction of ore-stage magnetite with meteoric fluids. Rhodes and Oreskes (1999) concluded that both textural types of magnetite, after filtering the data to remove hematite-bearing analyses, crystallized from the same ore fluid. Those authors also measure the oxygen isotope compositions of the whole-rock andesite that hosts the orebodies, diopside from altered andesite host rock, apatite separated from apatite-magnetite intergrowths from the orebodies, and quartz from hydrothermal magnetite-quartz veins. Their reported $\delta^{18}O$ values for andesite host rock increase with increasing degree of hydrothermal alteration, and the $\delta^{18}O$ values for diopside, apatite, and quartz are heavier than expected if those minerals crystallized from silicate melt. Rhodes and Oreskes (1999) interpreted the $\delta^{18}O$ data to indicate that the bulk of the magnetite at El Laco precipitated from an $^{18}O$-enriched hydrothermal fluid that metasomatically replaced andesitic lava flows; i.e., magnetite did not crystallize from silicate melt. Such metasomatic replacement by an isotopically heavy fluid was invoked as the cause of the isotopic enrichment of silicate minerals, apatite, and host whole-rock.

Nyström et al. (2008) sampled magnetite from the same orebodies as Rhodes and Oreskes (1999) and reported a mean $\delta^{18}O \pm 2\sigma$ value of 3.0 ± 1.2‰ and a total range of $\delta^{18}O$ values from 2.3 to 4.2‰ ($n$ = 14; Fig. 5). Contrary to Rhodes and Oreskes (1999), Nyström et al. (2008) reported that, when categorized by their respective magmatic and hydrothermal textures, the $\delta^{18}O$ values for "magmatic" magnetite at San Vicente Bajo yielded a mean $\delta^{18}O$ value of 3.7‰ and "hydro-

Table 2. Samples from Rodados Negros Analyzed for $\delta^{17}O$ and $\delta^{18}O$ with Calculated $\Delta^{17}O$ (eq. 2)

| Sample | $\delta^{17}O$ (‰) | $\delta^{18}O$ (‰) | $\Delta^{17}O$ (‰) |
|---|---|---|---|
| RN-1 | 1.46 | 2.99 | –0.13 |
| RN-2 | 1.83 | 3.61 | –0.09 |
| RN-3 | 1.89 | 3.69 | –0.07 |
| RN-4 | 1.76 | 3.53 | –0.11 |
| RN-5 | 1.74 | 3.42 | –0.07 |

Notes: Each sample was analyzed three times and the $2\sigma$ is ≤0.06‰ for both $\delta^{17}O$ and $\delta^{18}O$ for each sample

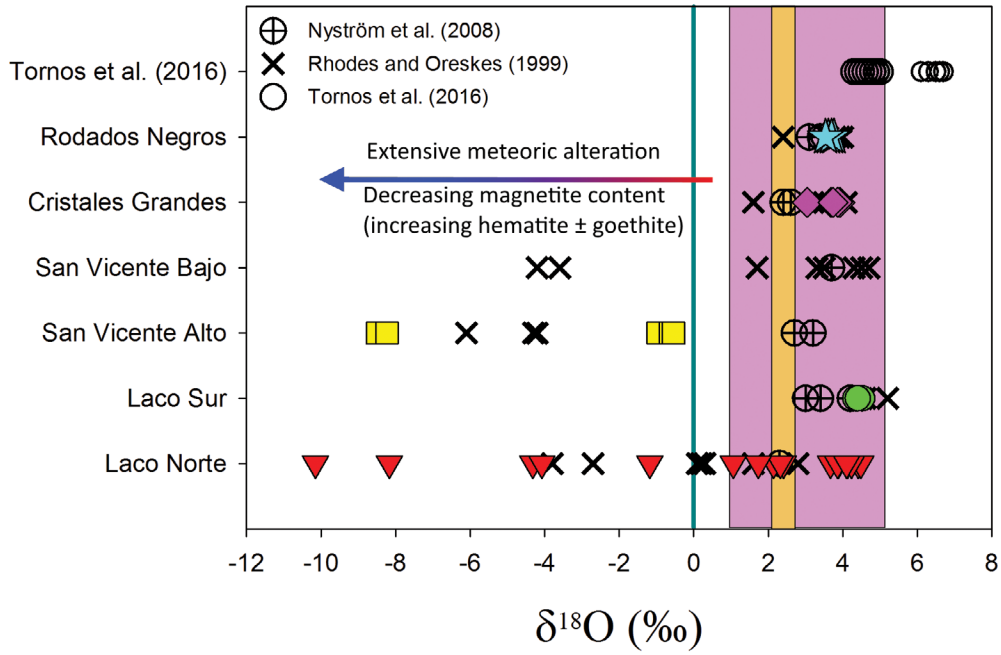


Fig. 5. Plot of $\delta^{18}O$ values for samples from Laco Norte, Laco Sur, Rodados Negros, Cristales Grandes, and San Vicente Alto, and from previous studies. Blue line denotes seawater (0‰), orange band denotes magnetite in equilibrium with MORB (2.2–2.6‰), and pink band denotes magnetite in equilibrium with typical continental magmas (~1–5‰; Taylor, 1967, 1968; Bindeman 2008).

thermal" magnetite intergrown with pyroxene in veins at Cristales Grandes yielded a mean $\delta^{18}O$ value of 2.4‰. Nyström et al. (2008) also quantified the modal abundance of hematite in their samples, but their data do not reveal the same systematic relationship between decreasing $\delta^{18}O$ values and increasing hematite content as reported by Rhodes and Oreskes (1999). Nyström et al. (2008) reported that the range of $\delta^{18}O$ values in magnetite from "magmatic-textured ore" overlaps the range of $\delta^{18}O$ values reported for magnetite from igneous rocks (i.e., $\delta^{18}O$ = 1–4‰; Taylor, 1967, 1968). Nyström et al. (2008) interpreted the small range of $\delta^{18}O$ values, which overlap those reported by Rhodes and Oreskes (1999), and the statistically different mean $\delta^{18}O$ values for magmatic- and hydrothermal-textured magnetite to indicate that all of the orebodies at El Laco share a common source. Those authors proposed that the magmatic-textured magnetite crystallized from a cooling Fe-rich magma, whereas the slightly lower mean $\delta^{18}O$ values for hydrothermal-textured vein magnetite at Cristales Grandes (as low as 2.3‰) resulted from magnetite growth from a magmatic-hydrothermal fluid that exsolved from the Fe-rich magma.

The $\delta^{18}O$ values reported in the current study are consistent with those reported in Rhodes and Oreskes (1999) and Nyström et al. (2008) (Fig. 5). Collectively, the data indicate that magnetite from the El Laco orebodies yield a very narrow range of $\delta^{18}O$ values when the data set is filtered for samples that clearly have been affected by syn- or postmineralization alteration; i.e., hematite and/or goethite are present (Figs. 4a, 5, 6, 7). The $\delta^{18}O$ data reported here and in published studies overlap $\delta^{18}O$ values reported for magnetite from igneous rocks and magmatic-hydrothermal systems (Taylor, 1967, 1968; Bilenker et al., 2016; Fig. 5). High temperatures of mineralization in the El Laco orebodies are also indicated by homogenization temperatures above 800°C of primary fluid inclusions hosted in clinopyroxene phenocrysts intimately intergrown with magnetite at Laco Sur and Cristales Grandes (Broman et al., 1999). Sheets et al. (1997) found that primary fluid inclusions in apatite and clinopyroxene contained hematite and anhydrite daughter crystals and have homogenization temperatures that cluster in two ranges of 710° to 750° and 830° to 840°C. Sheets et al. (1997) reported that primary fluid inclusions hosted in apatite coeval with magnetite exhibit variable phase ratios and salinities from 0.2 to 59 wt % NaCl equiv. Those observations suggest trapping of fluid inclusions in a boiling system, which is consistent with the range of $\delta^{18}O$ values (7.1–27.9‰) reported by Rhodes and Oreskes (1999) for quartz sampled from hydrothermal magnetite-quartz veins. The fluid inclusion data evince that high-temperature fluid was present during the formation of the magnetite-rich orebodies at El Laco.

The $\delta^{18}O$ values discussed above for magnetite ore samples from El Laco can be used with $\delta^{18}O$ values (7.2–7.9‰) for unaltered (or least altered) andesite whole rock from El Laco reported by Rhodes and Oreskes (1999) to calculate equilibrium temperatures for magnetite-andesite pairs. Based on the fractionation factors reported by Zhao and Zheng (2003), magnetite will yield $\delta^{18}O$ values from 3 to 5‰ if it crystallized at temperatures between 700° and 900°C from andesitic melt with the $\delta^{18}O$ composition measured by Rhodes and Oreskes (1999). This predicted range of $\delta^{18}O$ values for magnetite encompasses the majority of unaltered magnetite samples from all five orebodies in the current and previous studies of El Laco. By comparison, the global range of $\delta^{18}O$ values of typical magmatic waters is 5.5

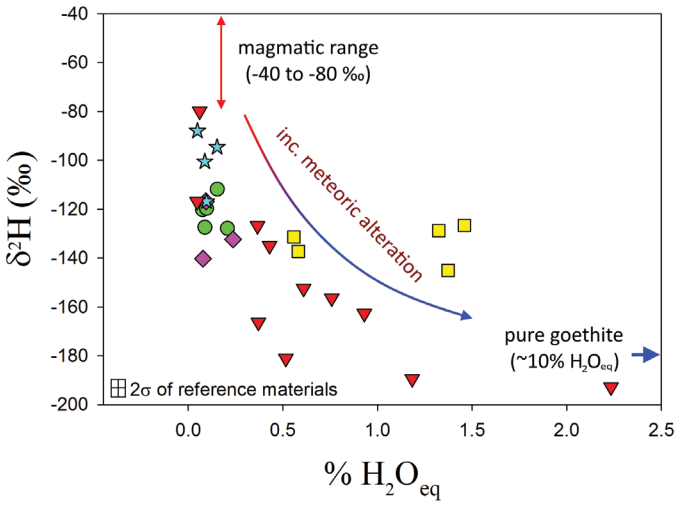


Fig. 6. Plot of $\delta^2H$ and measured $H_2O_{equiv}$ contents of hydrogen in iron oxides from Laco Norte, Laco Sur, Rodados Negros, Cristales Grandes, and San Vicente Alto (same legend as Fig. 3). Samples analyzed from these deposits show a clear trend from magmatic values, with increasing meteoric alteration where Laco Norte and San Vicente Alto show the highest degree of alteration of magnetite to goethite, incorporating more meteoric H. Magmatic range from Taylor and Epstein (1966). Precision on data points at $H_2O$ <0.15 wt % is likely ±20‰.

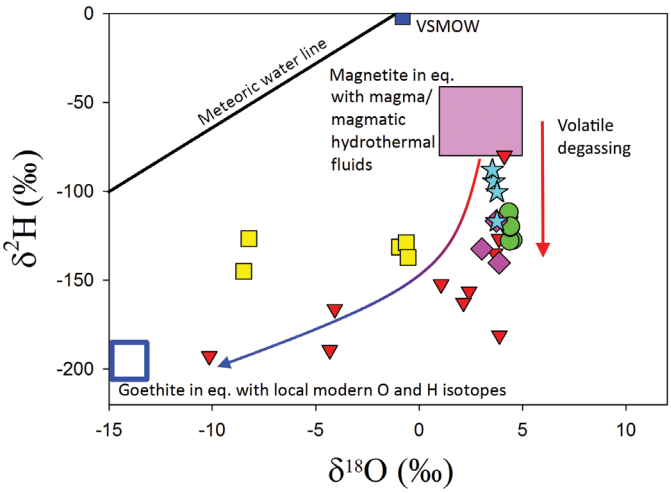


Fig. 7. Plot of $\delta^{18}O$ and $\delta^2H$ from iron oxides from Laco Norte, Laco Sur, Rodados Negros, Cristales Grandes, and San Vicente Alto (same legend as Fig. 3). Samples show a degassing trend in samples from Laco Sur, Rodados Negros, and Cristales Grandes, and a clear trend from magmatic values to meteoric values, where Laco Norte and San Vicente Alto show highest degree of alteration of magnetite to goethite, approaching equilibrium with modern-day meteorically derived goethite (Waterisotopes, 2018). Magmatic range from Taylor (1974). Error bars are smaller than icons.

to 10‰ (Taylor, 1967, 1968), which could result in magmatic-hydrothermal magnetite with $\delta^{18}O$ values between 0 and 5‰ at 800°C, consistent with the fluid inclusion homogenization temperatures reported by Sheets (1997) and Broman et al. (1999). The predicted $\delta^{18}O$ values for magnetite and comparison to $\delta^{18}O$ values for magnetite from igneous and magmatic-hydrothermal systems indicates that the $\delta^{18}O$ values for magnetite from El Laco overlap $\delta^{18}O$ values for magnetite crystallized from silicate melt (i.e., magmatic magnetite) and magnetite crystallized from magmatic-hydrothermal fluid (i.e., magmatic-hydrothermal magnetite). Importantly, the range of $\delta^{18}O$ values reported for unaltered magnetite cannot be used to discriminate between igneous and magmatic-hydrothermal magnetite.

In addition to the more traditional $\delta^{18}O$ values presented in this study, we also measured the abundance of $^{17}O$ in the least altered samples from Rodados Negros and used the calculated $\Delta^{17}O$ values (eq. 2) to assess the source reservoir(s) for oxygen in the magnetite (Pack et al., 2016; Miller et al., 2020; Fig. 8). Magnetite samples from Rodados Negros were chosen for this analysis based on their narrow ranges of $\delta^{56}Fe$ and $\delta^{18}O$ values and the lack of hematite and goethite. The $\Delta^{17}O$ values for the samples from Rodados Negros (Table 2), when plotted against corresponding $\delta^{18}O$ values for the same samples, are consistent with the oxygen isotope signature of mantle-derived silicate minerals (Pack et al., 2016; Miller et al., 2020; Fig. 8). The oxygen isotope data, when plotted in $\Delta^{17}O$ and $\delta^{18}O$ space plot lower than the mantle, do not lie along the trend connecting it to the meteoric water line, as would be expected if meteoric or basinal fluids had been involved in mineralization. Thus, the sum of the oxygen isotope data fingerprint a silicate magma source for oxygen but cannot discriminate between a silicate melt or magmatic-hydrothermal fluid as the ore fluid and require an additional low $\Delta^{17}O$ fluid. Our data are very similar to data from the Iranian Yazd and Sirjan IOA deposits presented by Peters et al. (2019), who suggest ore-fluid interaction with local evaporites may contribute to low $\Delta^{17}O$ values. This is a plausible explanation for El Laco, since non-marine evaporites are abundant in northern Chile, as pointed out by Rhodes and Oreskes (1999).

### *Iron isotopes constraints on the source reservoir for the El Laco ore fluid*

The iron stable isotope system is relatively new as a tool in geologic systems compared to conventional stable isotope systems such as $\delta^{18}O$, $\delta^2H$, and $\delta^{34}S$ (Dauphas et al., 2017 and references therein). Iron isotope abundances in iron oxide minerals are more resistant to secondary alteration than are the abundances of hydrogen and oxygen (Frost et al., 2007; Weis, 2013; Bilenker et al., 2016; Childress et al., 2016, 2020; Troll et al., 2019), and will only significantly deviate from their original signature (i.e., to lighter values) via extensive coupled dissolution-reprecipitation reactions with hydrothermal fluids, as has been reported for the Mineville IOA deposit (U.S.A.; Bilenker et al., 2016) and the Dannemora (Sweden; Weis, 2013) and Chagangnuoer (China; Günther et al., 2017) iron skarn deposits (Fig. 9). The $\delta^{56}Fe$ values for magnetite and iron oxide samples from the five El Laco orebodies investigated in the current study range from 0.04 to 0.70‰, with the greatest variation observed among samples from San Vicente Alto (0.15‰, 2$\sigma$) and the lowest variation among samples from Rodados Negros (0.02‰, 2$\sigma$; Table 1). The $\delta^{56}Fe$ values, when plotted against the $\delta^{18}O$ values for the same samples (Fig. 9) reveal that the majority of $\delta^{56}Fe$ and $\delta^{18}O$ values lie within the established range reported for magnetite that crystallized from silicate melt (i.e, magmatic) or magmatic-hydrothermal fluid (cf. Simon et al., 2018; Troll et al., 2019). The $\delta^{56}Fe$ values do not distinguish magmatic magnetite from magmatic-hydrothermal magnetite

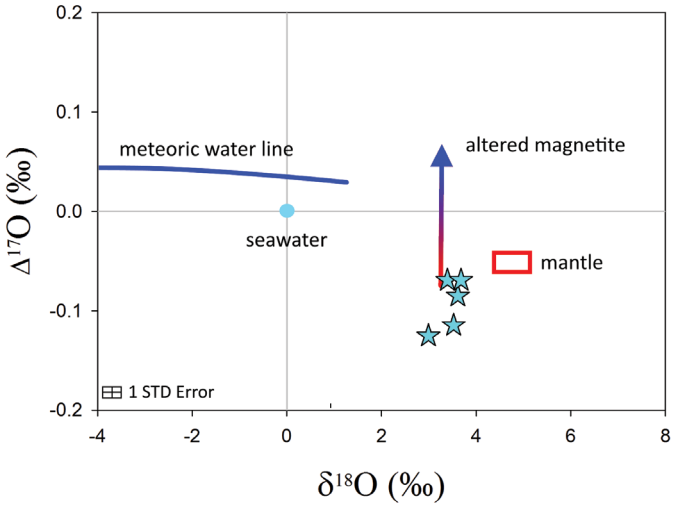


Fig. 8. Plot of $\delta^{18}O$ and $\Delta^{17}O$ for magnetite from Rodados Negros from this study. Blue dot denotes average value of seawater, blue line is the meteoric water line, and the red box is typical mantle silicate values as measured by Pack et al. (2016) and Miller et al. (2020). Samples analyzed from Rodados Negros clearly exhibit magmatic values with an unknown low-$\Delta^{17}O$ influence. Ore-fluid interaction with low-$\Delta^{17}O$ local non-marine evaporites offers a plausible explanation, as originally suggested by Rhodes and Oreskes (1999).

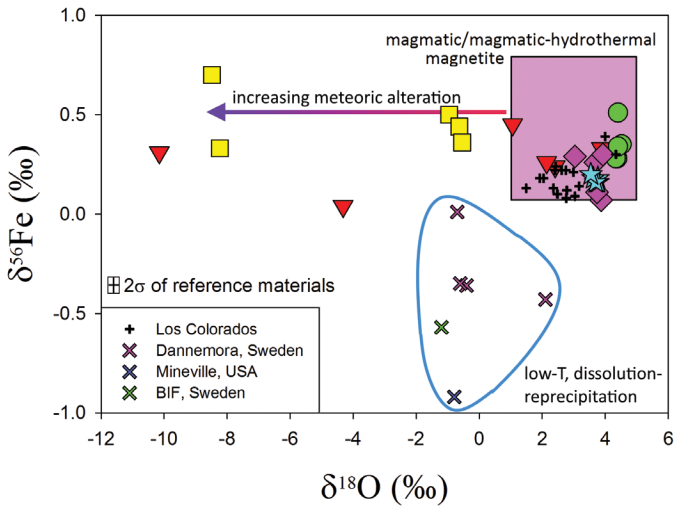


Fig. 9. Plot of $\delta^{18}O$ and $\delta^{56}Fe$ from iron oxides from Laco Norte, Laco Sur, Rodados Negros, Cristales Grandes, and San Vicente Alto (same legend as Fig. 3). The majority of samples from this study plot within the magmatic range, similar to the Los Colorados deposit (Bilenker et al. 2016). Laco Norte and San Vicente Alto trend toward lower $\delta^{18}O$ values, indicating higher degrees of alteration. Low-temperature and dissolution-reprecipitation-derived magnetite will commonly exhibit low $\delta^{56}Fe$ values. Magmatic range and additional data from Taylor (1974), Weis (2013), and Bilenker et al. (2016, 2017).

but do fingerprint a silicate magma source for iron in the El Laco orebodies, consistent with the $\delta^{18}O$ and $\Delta^{17}O$ discussed above. Importantly, the iron and oxygen stable isotope data exclude meteoric and basinal fluids as the primary ore-forming fluid in the El Laco system (Bilenker et al., 2016; Simon et al., 2018; Troll et al., 2019).

### *Hydrogen and oxygen isotopes constrain meteoric water alteration of magnetite*

The occurrence of hematite and goethite in magnetite from the El Laco orebodies has been interpreted to reflect hydrothermal alteration of magnetite by meteoric waters. Rhodes et al. (1997, 1999), and Rhodes and Oreskes (1999) suggest that the orebodies themselves could be the result of metasomatic replacement of andesite lava flows by Fe-rich basinal brines or perhaps fluids from nearby saline lakes or buried evaporites in accordance with the evaporite fluid source model of Barton and Johnson (1996). To test both of these hypotheses, we measured $^{1}H$ and $^{2}H$ abundances in magnetite and iron oxide samples from all five orebodies and report the first $\delta^{2}H$ data for magnetite and iron oxides from El Laco (Table 1). Hydrogen in magnetite may be present in fluid inclusions, hydrogen in goethite (FeO(OH)), or a combination of both. The analyzed samples yield $\delta^{2}H$ values that range from –193 to –80‰ (Table 1; $n$ = 28), where Laco Norte exhibits the greatest range (140‰) and samples from the other four orebodies yield smaller ranges (≤29‰). The $\delta^{2}H$ values for typical magmatic waters range from about –40 to –0‰ (Taylor, 1974; Dixon et al., 2017) and $\delta^{2}H$ and $\delta^{18}O$ values for local, modern meteoric waters range from about –106 to –70.5 and –15.1 to –12.8‰, respectively (Waterisotopes Database, 2018), where lighter values correspond to higher elevation. For reference, goethite in equilibrium with the isotopically lightest modern meteoric waters will yield $\delta^{2}H$ and $\delta^{18}O$ values of –211 and –15.4‰ at 25°C, respectively (Yapp and Pedley, 1985; Müller, 1995). Magnetite and iron oxide samples from Laco Norte and San Vicente Alto yield $\delta^{2}H$ and $\delta^{18}O$ values that become progressively lighter with increasing modal abundance of goethite (Fig. 7), which is expected if goethite is the result of meteoric water alteration of magnetite. The latter is corroborated by the systematic increase of the measured $H_2O$ equiv content of samples from Laco Norte and San Vicente Alto (Fig. 6), with a maximum of 2.2% $H_2O$ equiv (pure goethite = ~10% $H_2O$ equiv) corresponding to the lightest $\delta^{2}H$ and $\delta^{18}O$ values in this study (sample LN-2 from Laco Norte) in the most altered samples from Laco Norte.

For magnetite samples from Laco Sur, Rodados Negros, and Cristales Grandes, $\delta^{2}H$ values range from –88 to –140‰ as $\delta^{18}O$ values vary from 3.5 to 4.5‰. This observation requires a process that causes a much larger fractionation of hydrogen isotopes compared to oxygen isotopes. The oxygen and iron stable isotopes discussed above fingerprint a silicate magma as the source of both of those elements in magnetite in the El Laco orebodies. In silicate magmas, saturation of silicate melt with a magmatic-hydrothermal volatile phase results in strong fractionation of $^{2}H$ into the vapor phase, and open-system degassing decreases the $\delta^{2}H$ value of the residual silicate melt (Taylor et al., 1983; Hedenquist and Lowenstern, 1994). The $\delta^{2}H$ values of fluid inclusions trapped in magnetite that crystallizes from a silicate melt experiencing open-system degassing will become progressively more negative. Considering that the effect of volatile loss on oxygen isotope fractionation in a silicate magma is very small relative to its effect on hydrogen isotope fractionation (Hedenquist and Lowenstern, 1994), the $\delta^{18}O$ values for magnetite crystallized from a degassing melt will exhibit a much smaller range relative to $\delta^{2}H$. Thus, the $\delta^{2}H$ and $\delta^{18}O$ data for magnetite from Laco

Sur, Rodados Negros, and Cristales Grande can plausibly be explained by magnetite crystallization in an open-system degassing silicate magma. Another plausible explanation for the large range of $\delta^2H$ values for magnetite at nearly constant $\delta^{18}O$ values is crystallization of magnetite from hydrothermal fluid that experiences phase separation (i.e., boiling) and loss of a vapor during decompression. Horita and Wesolowski (1994) reported that $^2H$ preferentially partitions into the vapor during boiling above 250°C, whereas the $\delta^{18}O$ value of liquid and vapor are almost identical above 250°C. In that scenario, the $\delta^2H$ values of magnetite that crystallizes from a boiling aqueous liquid that is boiling will progressively decrease at nearly constant $\delta^{18}O$. At El Laco, Rhodes and Oreskes (1999) reported that boiling is a plausible explanation for the range of $\delta^{18}O$ values for hydrothermal quartz, and Sheets et al. (1997) invoked boiling to explain the range of salinities and phase ratios in fluid inclusions trapped in apatite and clinopyroxene coeval with magnetite in the El Laco orebodies. We suggest that rather than distinguishing between a purely magmatic and purely hydrothermal origin for the magnetite-rich orebodies at El Laco, which cannot be done with the $\delta^2H$, $\delta^{18}O$, and $\delta^{56}Fe$ data presented in the current and published studies, a unifying genetic model that combines magmatic and magmatic-hydrothermal processes is necessary. We present and discuss such a model below, but first used the oxygen isotope data presented here and in published studies to evaluate the hypothesis that the El Laco orebodies formed by liquid immiscibility.

*Testing the liquid immiscibility hypothesis*

One of the proposed genetic models for the formation of El Laco and other IOA deposits invokes unmixing of a silicate melt into immiscible Fe-P-rich, Si-poor melt and conjugate Fe-poor, Si-rich melt (Philpotts, 1967; Naslund et al., 2002; Tornos et al., 2016; Velasco et al., 2016; Hou et al. 2018). Proponents of the liquid immiscibility model cite the presence of what are interpreted to be Fe- and P-rich globules hosted exclusively in silicate melt inclusions within pyroxene and plagioclase phenocrysts in the andesite host rocks (Naslund et al., 2009; Tornos et al., 2016; Velasco et al., 2016). Tornos et al. (2016) reported stable $\delta^{18}O$ values for the andesite host (7.4–9.6‰), stratabound magnetite from Laco Sur (4.3–5.0‰), and magnetite from a diopside-magnetite-anhydrite vein (4.4–6.7‰; Fig. 5). The $\delta^{18}O$ values reported by those authors generally agree with data reported in the current study as well as Rhodes and Oreskes (1999) and Nyström et al. (2008), with the exception of heavier $\delta^{18}O$ values in magnetite from the diopside-magnetite-anhydrite vein. Tornos et al. (2016) used $\delta^{18}O$ values of coexisting magnetite and diopside from a vein that crosscuts the host andesite to calculate a temperature range of 900° to 1,300°C, with most calculated temperatures in the range 900° to 1,125°C, based on the diposide-magnetite geothermometer of Matthews et al. (1983). A temperature of 1,300°C is hotter than any known shallow-level crustal igneous system except for the eruption of ultramafic lavas known as komatiites that erupted predominantly in the Proterozoic and Archean (Condie et al., 2016). Tornos et al. (2016) pointed out that experimental studies demonstrate that water-saturated andesite melt at low pressure crystallizes over the temperature range 1,030° to 950°C (Moore and Carmichael, 1998; Blundy et al., 2006), and that the $\delta^{18}O$ values they determined for magnetite and host andesite from El Laco are consistent with magnetite that crystallized in equilibrium with andesite melt over a temperature range of 650° to 1,350°C. The liquid immiscibility hypothesis that invokes crystallization of the magnetite-rich orebodies from an Fe- and P-rich liquid in equilibrium with host andesite at El Laco can be tested directly by using experimental data that constrain the partitioning of O isotopes between immiscible Si- and Fe-rich melts over the temperature range at which andesites crystallize.

Kyser et al. (1998) demonstrated experimentally at 1,180°C and 0.1 MPa that O isotopes only slightly fractionate between Si-rich melt and conjugate Fe-rich melt that form by unmixing of an initial silicate melt in the $Fe_2SiO_4$-$KAlSi_2O_6$-$SiO_2$ system. Those authors report a $\Delta^{18}O$ value, which is defined as $\delta^{18}O_{Si\text{-}rich\text{-}melt}$- $\delta^{18}O_{Fe\text{-}rich\text{-}melt}$, of 0.5 to 0.6‰. Lester et al. (2013b) performed experiments at 1,100° to 1,200°C to quantify O isotope fractionation between Si- and Fe-rich melts and reported $\Delta^{18}O$ values that vary between ~0.0 and 0.5‰, in agreement with the values reported by Kyser et al. (1998). These experimentally constrained fractionation factors for O isotopes in Si-rich and conjugate Fe-rich melts indicate that the iron oxide orebodies at El Laco should yield $\delta^{18}O$ values of ~7 to 9‰ if the orebodies crystallized from Fe-rich melt that had been in equilibrium with andesite host rocks, even when projected to lower temperatures. However, unaltered magnetite at El Laco yields $\delta^{18}O$ values of ~3.5 to 5‰, as reported in the current study as well as in Rhodes and Oreskes (1999) and Tornos et al. (2016). The $\delta^{18}O$ values for magnetite at El Laco are entirely consistent with the range of typical igneous and magmatic-hydrothermal magnetite (cf. Taylor, 1967; Loewen and Bindeman, 2016; Fig. 5).

Lester et al. (2013a) performed experiments in the systems $Fe_2SiO_4$-$Fe_3O_4$-$KAlSi_2O_6$-$SiO_2$, $Fe_3O_4$-$KAlSi_2O_6$-$SiO_2$, and $Fe_3O_4$-$Fe_2O_3$-$KAlSi_2O_6$-$SiO_2$ at temperatures of 1,075° to 1,200°C at 200 MPa and oxygen fugacities ($f_{O_2}$) within the magnetite stability field to assess the possible effects of $H_2O$ alone or $H_2O$ in combination with P, S, F, and Cl on liquid immiscibility. Importantly, the authors added 10% $H_2O$ by mass to their experiments and did not measure the $H_2O$ content of the quenched immiscible Si- and Fe-rich liquids. The authors did quantify and report that P, S, and Cl partition preferentially into the Fe-rich immiscible liquid, with P and S strongly preferring the Fe-rich melt and F showing equal preference for the Fe- and Si-rich melts. Their results indicate that the addition of $H_2O$ along with P, S, and F (not Cl) decreases the temperature at which liquid immiscibility occurs and expands the compositional ranges of the two-liquid field. On the contrary, the addition of only $H_2O$ and Cl resulted in formation of a single melt at all conditions except one experiment at 1,200°C. Lester et al. (2013b) reported that the addition of only $H_2O$ and Cl increases the activity of Si in the melt, hence the temperature of the silicate mineral saturation surface, which prevents unmixing of the silicate liquid. Based on their experimental results for a hydrous assemblage and the experimental results of Naslund (1983) for anhydrous assemblages, liquid immiscibility is not expected to occur below temperatures of ~1,075°C at $f_{O_2}$ of MH or ~1,100°C at $f_{O_2}$ NNO and, critically, is not expected to occur in systems with $H_2O$ + Cl.

Broman et al. (1999) reported data for fluid inclusions hosted in pyroxene intergrown with magnetite at Laco Sur and from a vein crosscutting ore breccia in a dike-vein system at Cristales Grandes that reveal the ore-associated fluids (interpreted by those authors as having exsolved from the Fe magma after emplacement and crystallization) are Na-K chloride rich and contain anhydrite daughter crystals. They refer to the inclusions as "hydrous saline melt" and report that the inclusions homogenize at >800°C. Broman et al. (1999) interpreted the presence of the Na-K-Cl inclusions as evidence for exsolution of a hydrous saline melt from a decompressing magma, consistent with the studies of Cline and Bodnar (1991) and Webster (1997). In light of the experimental study of Lester et al. (2013b) described above, the Cl-rich nature of the inclusions seems inconsistent with the liquid immiscibility hypothesis.

Most recently, Hou et al. (2018) used Raman spectroscopy to measure the $H_2O$ concentration of experimentally produced conjugate Fe- and Si-rich melts in a Cl-free $SiO_2$- $TiO_2$-$Al_2O_3$-$Fe_2O_3$-FeO-MnO-MgO-$CaF_2$ assemblage. Hou et al. (2018) reported that $H_2O$ preferentially partitions into the Si-rich melt, with Si-melt/Fe-melt partition coefficients that vary from 1.4 to- 2.5. This finding demonstrates that even if liquid immiscibility did occur in a Cl-rich system, which is the opposite of what Lester et al. (2013b) determined experimentally, the addition of $H_2O$ to the Si-rich melt will lower its bulk density relative to its conjugate Fe-rich melt such that the Fe-rich melt gravitationally sinks and the Si-rich melt buoyantly ascends. The liquid immiscibility hypothesis invoked by Tornos et al. (2016) to explain the eruption of Fe-rich magma at El Laco requires $H_2O$ to partition preferentially into the Fe-rich melt during liquid-liquid unmixing, such that the Fe-rich melt is less dense than its conjugate Si-rich melt and can ascend buoyantly from the source magma. Thus, the experimental results of Hou et al. (2018) falsify the liquid immiscibility hypothesis as proposed by Tornos et al. (2016).

In summary, the experimental data that constrain the partitioning of oxygen isotopes between conjugate Fe- and Si-rich melts demonstrate that liquid immiscibility does not occur in $H_2O$ + Cl-bearing silicate melts and appears to disallow liquid immiscibility as a plausible explanation for mineralization at El Laco.

### *The origin of the El Laco magnetite-rich orebodies*

The $\delta^{56}$Fe, $\delta^{18}$O, and $\Delta^{17}$O stable isotope data presented in this paper fingerprint a silicate magma as the source of oxygen and iron in magnetite in the El Laco orebodies. As discussed above, the $\delta^{56}$Fe and $\delta^{18}$O values for unaltered magnetite from the El Laco orebodies overlap values for magnetite from igneous rocks and magmatic-hydrothermal systems. The overlap of stable isotope values for magmatic- and hydrothermal-textured magnetite indicates that the data cannot be used to discriminate magnetite that crystallized from silicate melt from magnetite that crystallized from magmatic-hydrothermal fluid. Published fluid inclusion data indicate that chlorine-rich high-temperature fluids, i.e., >700°C, were involved in the genesis of the orebodies (Sheets et al., 1997; Broman et al., 1999). Studies of magnetite chemistry from outcrop and drill core samples reveal that the trace element concentrations of magnetite systematically increase with depth in the orebodies, where magnetite from deep samples has igneous-like compositions, and magnetite at intermediate to shallow depths has compositions that overlap magmatic-hydrothermal magnetite (Ovalle et al., 2018; La Cruz, 2020). For example, the concentration of titanium in magnetite systematically increases from about 0.2 wt % in surface samples to ~0.76 wt % at 188-m depth, and titanomagnetite crystals at 188 m exhibit triple junctions and trellis-textured ilmenite exsolution lamellae that are hallmark characteristics for igneous magnetite equilibrated with magmatic-hydrothermal fluid (Ovalle et al., 2018).

Ovalle et al. (2018) proposed a new genetic model for the El Laco orebodies that explains the systematic variability of trace element concentrations in unaltered magnetite, the near-magmatic to magmatic fluid inclusion homogenization temperatures, and the observation of magmatic- and hydrothermal-textured magnetite. Ovalle et al. (2018) propose that the El Laco orebodies form by a combination of igneous and magmatic-hydrothermal processes (Fig. 10), wherein the igneous-like (Ti-rich) magnetite at intermediate to deep levels of the orebodies crystallized from silicate melt. As demonstrated experimentally and by thermodynamic modeling (Knipping et al., 2019b), magnetite is the liquidus phase in oxidized, water-rich andesitic magma. Volatile saturation of magnetite-saturated andesitic melt results in magmatic-hydrothermal fluid bubbles that nucleate preferentially on magnetite crystal faces that have diameters on the order of tens to a few hundred microns (Hurwitz and Navon, 1994; Knipping et al., 2019b). Iron and chlorine efficiently partition from silicate melt to magmatic-hydrothermal fluid as $FeCl_2$, and iron is the most abundant cation in said fluid, obtaining concentrations of tens of wt % Fe (Simon et al., 2004; Bell and Simon, 2011). Rapid decompression of the magma during, for example, collapse of the El Laco volcano edifice, results in the formation of a magnetite-fluid suspension that behaves as a discrete phase within the magma chamber (Knipping et al., 2019b). The magnetite-fluid suspension has a lower bulk density than the surrounding magma as long as the volume fraction of magnetite microlites is less than 37% (Knipping et al., 2015a) and will buoyantly ascend through the magma during edifice collapse. Geologically instantaneous destabilization of a magma body during edifice collapse results in rapid transport (5–20 m/s) through hydraulic fractures that evolve in a ductile crystal-mush regime (Hautmann et al., 2014), wherein high-flux permeable channels become well developed with increasing crystallinity (cf. Hersum et al., 2005).

Rapid ascent of the magnetite-fluid suspension and hydraulic injection of the magnetite-rich suspension through fissures formed during edifice collapse, will form large hydrothermal breccia bodies characterized by a matrix of an aggregate of primary igneous magnetite (Ovalle et al., 2018). Hydrothermal-textured magnetite will precipitate from the ascending and surface-venting iron-rich magmatic-hydrothermal fluid owing to the decrease of magnetite solubility with decompression and cooling. During decompression, the magmatic-hydrothermal fluid will boil, which explains the progressively lighter $\delta^2$H values of unaltered magnetite at the nearly constant $\delta^{18}$O values reported here, as well as the range of $\delta^{18}$O values reported for hydrothermal quartz (Rhodes and Oreskes, 1999), and the range of salinities and phase ratios in fluid inclusions

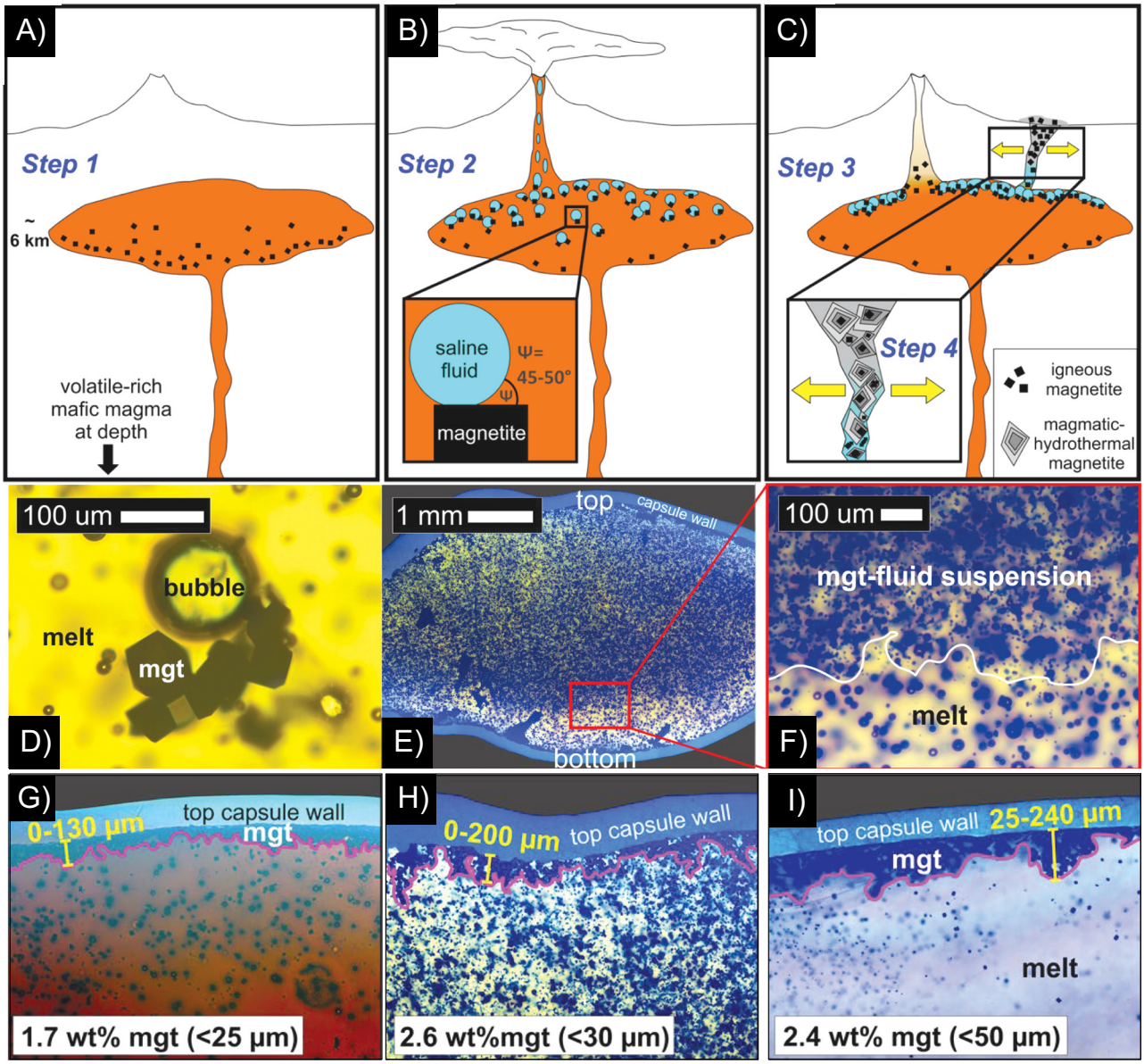


Fig. 10. Schematic illustration of the genetic model proposed by Ovalle et al. (2018) for the formation of the El Laco orebodies. (A). Igneous magnetite crystallizes from andesitic melt in a magma reservoir, followed by (B) exsolution of an iron-rich magmatic-hydrothermal fluid that nucleates on igneous magnetite (mgt) microlites, forming a magnetite-fluid suspension that (C) buoyantly coalesces and ascends to form a magnetite-fluid suspension that accumulates at the top magma chamber. Collapse of the volcanic edifice causes the magnetite-fluid suspension to experience rapid decompression during ascent, emplacement, and surface-venting along permeable structures within the magma chamber and in the superjacent crust (C). Experimental observations demonstrate that igneous magnetite is wetted by a magmatic-hydrothermal fluid that exsolves from andesitic melt (D), and that the resulting magnetite-fluid suspension coalesces and ascends buoyantly through the magma during decompression. (E) through (I) show the formation of a magnetite-fluid layer that forms at the top of andesitic magma after decompression from 250 to 150 MPa at a constant temperature of 1,050°C and oxygen fugacity of ~NNO + 3. (G). Magnetite-fluid layer quenched immediately after decompression, (H) after holding the experiment for 3 h after decompression, and (I) after holding the experiment for 72 h after decompression. Modified from Knipping et al. (2019b).

trapped in apatite and clinopyroxene coeval with magnetite in the orebodies. Boiling of the magnetite-fluid suspension during rapid emplacement and surface venting also explains the presence of cavities and gas escape tubes in surface outcrops originally described by Park (1961). The presence of clinopyroxene that contains primary fluid inclusions with homogenization temperatures >800°C is consistent with the presence of igneous clinopyroxene as a modally minor phase in the original igneous magnetite-fluid suspension. This is consistent with the experimental study of Pleše et al. (2018) who demonstrated that clinopyroxene is wetted by magmatic-hydrothermal fluid that exsolves from andesitic melt during decompression. Pleše et al. (2018) reported that heterogeneous bubble nucleation on igneous clinopyroxene crystals in andesitic melt

may influence permeability development within magma and promote explosive volcanic eruptions. The presence in apatite, which is coeval with magnetite in the orebodies, of primary fluid inclusions with homogenization temperatures that cluster in the ranges 710° to 750° and 830° to 840°C is consistent with apatite growth from silicate melt and magmatic-hydrothermal fluid. Hurwitz and Navon (1994) demonstrated experimentally that apatite is wetted by magmatic-hydrothermal fluid as it exsolves from silicate melt, as has been demonstrated experimentally for magnetite (Knipping et al., 2019b) and clinopyroxene (Pleše et al., 2018). Apatite is a modally minor phase in the El Laco orebodies, which contain <1 wt % $P_2O_5$. Apatite grains with primary fluid inclusions trapped at temperatures >800°C are consistent with crystallization from fluid-saturated silicate melt, and apatite grains with fluid inclusions trapped at temperatures below the andesite solidus are consistent with crystallization from magmatic-hydrothermal fluid. Phosphorus is highly mobile in magmatic-hydrothermal fluid, with fluid/silicate melt partition coefficients for phosphorus ranging from 2 to 6 (Zajacz et al., 2008). Thus, growth of apatite from the magmatic-hydrothermal fluid during rapid decompression and boiling of the fluid would result in the fluid inclusion behavior reported by Sheets et al. (1997) and the growth of fluorapatite at high temperature as reported by La Cruz et al. (2020). Growth of magnetite from a cooling magmatic-hydrothermal fluid explains the systematic decrease in trace element concentrations in magnetite over several hundred vertical meters in the orebodies (Ovalle et al., 2018; La Cruz et al., 2020). This would also explain why hydrothermal textures are observed in the near-surface environment at El Laco, whereas the igneous textures of unaltered magnetite observed in drill core are consistent with shallow emplacement of a magnetite-bearing magmatic-hydrothermal fluid. In this case, the titanomagnetite would have crystallized from silicate melt in the parent magma chamber that evolved the magmatic-hydrothermal ore fluid. The well-developed trellis- and sandwich-textured ilmenite oxyexsolution lamellae observed in magnetite samples in drill core from intermediate to deeper levels of the orebodies are consistent with the genetic model proposed by Ovalle et al. (2018). The oxyexsolved ilmenite results from oxidation of titanomagnetite during cooling at temperatures above 600°C (Lindsley, 1962, 1963, 1991; Buddington and Lindsley, 1964; Haggerty, 1976, 1991; Tucker and O'Reilly, 1980). Oxidation of primary, magmatic titanomagnetite at high temperature—when diffusion rates are high—in the presence of a fluid phase also explains the formation of interstitial ilmenite reported by Ovalle et al. (2018). The presence of triple junctions among magnetite grains at El Laco plausibly reflects equilibration of magnetite with interstitial high-temperature ore fluid during or after emplacement, which also explains the presence of monazite, thorite, and Nb oxide inclusions in magnetite, monazite inclusions in apatite, and magnetite octahedra observed growing from the walls of cavities and gas escape tubes. The genetic model of Ovalle et al. (2018) predicts that magnetite in the El Laco orebodies should have $\delta^{18}O$ and $\delta^{56}Fe$ values consistent with growth from silicate melt and magmatic-hydrothermal fluid, as reported here and in published studies. The presence of sulfide-bearing magnetite-diopside-scapolite veins and late veinlets of gypsum-magnetite-pyrite that crosscut the main breccia bodies at depth (Ovalle et al., 2018) and the advanced argillic alteration at the surface (Sillitoe and Burrows, 2002) are explained by circulation and cooling of the interstitial magmatic-hydrothermal fluid after emplacement and formation of the massive magnetite-rich orebodies.

## Conclusions

Iron and oxygen (including $^{17}O$) stable isotope abundances in magnetite from the El Laco IOA deposit in northern Chile fingerprint a silicate magma as the source of those elements. Hydrogen and triple oxygen isotopes in magnetite in some samples from the Laco Norte and San Vicente Alto orebodies reveal alteration by meteoric water, consistent with increasing abundances of goethite and measured $H_2O$ contents in samples with lighter $\delta^{18}O$ and $\delta^{2}H$ values. The $\delta^{18}O$ values in unaltered magnetite samples from Laco Sur, Cristales Grandes, and Rodados Negros overlap $\delta^{18}O$ values for igneous and magmatic-hydrothermal magnetite. The $\Delta^{17}O$ values for unaltered magnetite samples from Rodados Negros are consistent with mantle-derived oxygen. The $\delta^{56}Fe$ values of unaltered magnetite from all five orebodies sampled in this study overlap with purely igneous magnetite $\delta^{56}Fe$ values and magnetite from other IOA deposits, such as the Los Colorados and Mariela (Ignacia) deposits in Chile, Pea Ridge and Pilot Knob in the United States, and Kiruna and Grängesberg in Sweden. Importantly, the $\delta^{56}Fe$ values preserve original, ore-stage values even in bulk iron oxide samples that contain hematite and goethite, where $\delta^{18}O$ and $\delta^{2}H$ values of the latter fingerprint alteration by meteoric water. While we emphasize that we were unable to sample the two deposits thought to mostly likely represent metasomatic replacement, San Vicente Bajo and Laquito, the stable isotope data presented here from five of the six major orebodies are consistent with the combined magmatic/magmatic-hydrothermal model proposed by Ovalle et al. (2018) to explain the magmatic and hydrothermal chemistry and textures of magnetite at El Laco. The stable isotope data presented here, when combined with published trace element and fluid inclusion data for samples from the El Laco orebodies, preclude the possibility that the ore fluids and iron responsible for mineralization at El Laco were derived from a nonmagmatic source. The stable oxygen isotope data also preclude formation of the magnetite-rich orebodies via liquid immiscibility. Future isotopic studies should focus on in situ studies of statistically significant populations of individual magnetite grains in order to assess isotopic fractionation between magmatic and hydrothermal magnetite, and/or fractionation related to the thermal gradient from depth to surface, and to assess and contextualize evidence of metasomatic replacement by iron oxides.

## Acknowledgments

TMC thanks the Society of Economic Geologists, the American Association of Petroleum Geologists, and the University of Michigan for providing funding, CAP Mining for providing access to El Laco and plentiful tea and coffee. We thank Dominique Weis for allowing us to perform the iron isotope measurements in her laboratory facilities at the University of British Columbia Pacific Centre for Isotopic Research. We thank two anonymous reviewers for their constructive reviews which greatly helped clarify points in this manuscript. ACS

acknowledges funding from NSF EAR grants 1250239 and 1264560. MR and FB acknowledge funding from Chile's Millennium Science Initiative (MSI) through Millennium Nucleus for Metal Tracing along Subduction grant NC130065, and FONDECYT grant 1140780 "Metallogenesis of the Mesozoic magmatic arc of northern Chile: Testing the IOCG connection using a multi-proxy geochemical approach." INB acknowledges support from NSF EAR grant 1822977.

## REFERENCES

Barton, M.D., and Johnson, D.A., 1996, Evaporitic-source model for igneous-related Fe oxide-(REE-Cu-Au-U) mineralization: Geology, v. 26, p. 259–262.

Bell, A., and Simon, A.C., 2011, Evidence for the alteration of the $Fe^{3+}/\Sigma Fe$ of silicate melt caused by the degassing of chlorine-bearing aqueous volatiles: Geology, v. 39, p. 499–502.

Bilenker, L.D., Simon, A.C., Reich, M., Lundstrom, C.C., Gajos, N., Bindeman, I., Barra, R., and Munizaga, R., 2016, Fe-O stable isotope pairs elucidate a high-temperature origin of Chilean iron oxide-apatite deposits: Geochimica et Cosmochimica Acta, v. 177, p. 94–104.

Bilenker, L.D., VanTongeren, J.A., Lundstrom, C.C., and Simon, A.C., 2017, Iron isotopic evolution during fractional crystallization of the uppermost Bushveld Complex layered mafic intrusion: Geochemistry Geophysics Geosystems, v. 18, doi:10.1002/ 2016GC006660.

Bindeman, I., 2008, Oxygen isotopes in mantle and crustal magmas as revealed by single crystal analysis: Reviews in Mineralogy and Geochemistry, v. 69, p. 445–478.

Bindeman, I.N., Kamenetsky, V.S., Palandri, J., and Vennemann, T., 2012, Hydrogen and oxygen isotope behaviors during variable degrees of upper mantle melting: Example from the basaltic glasses from Macquarie Island: Chemical Geology, v. 310, p. 126–136.

Bindeman, I.N., Zakharov, D., Palandri, J., Greber, N.D., Retallack, G.J., Hoffman, A., Dauphas, N., Lackey, J.S., and Bekker, A., 2017, Rapid growth of subaerial crust and the onset of a modern hydrologic cycle at 2.5 Ga: Nature v. 557, p. 545–548, doi:10.1038/s41586-018-0131-1.

Bindeman, I.N., Zakharov, D.O., Palandri, J., Greber, N.D., Dauphas, N., Retallack, G.J., and Bekker, A., 2018, Rapid emergence of subaerial landmasses and onset of a modern hydrologic cycle 2.5 billion years ago: Nature, v. 557(7706), p. 545–548.

Blundy, J., Cashman, K., and Humphreys, M., 2006, Magma heating by decompression-driven crystallization beneath andesite volcanoes: Nature, v. 443, p. 76–80, doi:10.1038/nature05100.

Broman, C., Nyström, J.O., Henríquez, F., and Elfman, M., 1999, Fluid inclusions in magnetite-apatite ore from a cooling magmatic system at El Laco, Chile: Geologiska Föreningen, v. 121, p. 253–267.

Buddington, A.F., and Lindsley, D.H., 1964, Iron-titanium oxide minerals and synthetic equivalents: Journal of Petrology, v. 5(2), p. 310–357.

Cline, J.S., and Bodnar, R., 1991, Can economic porphyry copper mineralization be generated by a typical calc-alkaline melt: Journal of Geophysical Research, v. 96, p. 8113–8126.

Childress, T.M., Simon, A.C., Day, W.C., Lundstrom, C.C., and Bindeman, I.N., 2016, Iron and oxygen isotope signatures of the Pea Ridge and Pilot Knob magnetite-apatite deposits, Southeast Missouri, USA: Economic Geology, v. 111, p. 2033–2044.

Childress, T.M., Simon, A.C., Reich, M., Barra, F., Arce, M., Lundstrom, C.C., and Bindeman, I.N., 2020, Formation of the Mantoverde iron oxide-copper-gold (IOCG) deposit, Chile: Insights from Fe and O stable isotopes and comparison to iron oxide-apatite (IOA) deposits: Mineralium Deposita, doi:10.1007/s00126-019-00936-x.

Condie, K.C., Aster, R.C., and van Hunen, J., 2016, A great thermal divergence in the mantle beginning 2.5 Ga: Geochemical constraints from greenstone basalts and komatiites: Geoscience Frontiers, v. 7, p. 543–553.

Craddock, P.R., and Dauphas, N., 2011, Iron isotopic compositions of geological reference materials and chondrites: Geostandards and Geoanalytical Research, v. 35, no. 1, p 101–123.

Dare, S.A.S., Barnes, S-J., and Beaudoin, G., 2015, Did the massive magnetite "lava flows" of El Laco (Chile) form by magmatic or hydrothermal processes? New constraints from magnetite composition by LA-ICP-M: Mineralium Deposita, v. 50, p. 607–617, doi:10.1007/s00126-014-0560-1.

Dauphas, N., John, S.G., and Rouxel, O., 2017, Iron isotope systematics: Reviews in Mineralogy and Geochemistry, v. 82, p. 415–510.

Dixon, J.E., Bindeman, I.N., Kingsley, R.H., Simons, K.K., Le Roux, P.J., Hajewski, T.R., Swart, P., Langmuir, C.H., Ryan, J.G., Walowski, K.J., Wada, I., and Wallace, P.J., 2017, Light stable isotopic compositions of enriched mantle sources: Resolving the dehydration paradox: Geochemistry, Geophysics, Geosystems, v. 18, p. 3801–3839, doi:10.1002/2016GC006743.

Frost, C.D., von Blanckenburg, F., Shoenberg, R., Frost, B.R., and Swapp, S.M., 2007, Preservation of Fe isotope heterogeneities during diagenesis and metamorphism of banded iron formation: Contributions to Mineral Petrology, v. 153, p. 211–235.

Frutos, J., and Oyarzun M., J., 1975, Tectonic and geochemical evidence concerning the genesis of El Laco magnetite lava flow deposits, Chile: Economic Geology, v. 70, p. 988–990.

Günther, T., Klemd, R., Zhang, X., Horn, I., and Weyer, S., 2017, In-situ trace element and Fe-isotope studies on magnetite of the volcanic-hosted Zhibo and Chagangnuoer iron ore deposits in the Western Tianshan, NW China: Chemical Geology, v. 453, p. 111–127.

Haggerty, S.E., 1976, Oxidation of opaque mineral oxides in basalts: Mineralogical Society of America, Reviews in Mineralogy, Oxide Minerals, v. Am 3, p. Hg-1–100.

——1991, Oxide textures—A mini-atlas, *in* Lindsley, D.H., ed., Oxide minerals: Petrologic and magnetic significance: Reviews in Mineralogy, v. 25, p. 129 –137.

Hautmann, S., Witham, F., Christopher, T., Cole, P., Linde, A.T., Sacks, S., and Sparks, S.J., 2014, Strain field analysis on Montserrat (W.I.) as tool for assessing permeable flow paths in the magmatic system of Soufriere Hills Volcano: Geochemistry Geophysics Geosystems, v. 15, p. 676–690.

Hedenquist, J.W., and Lowenstern, J.B., 1994, The role of magmas in the formation of hydrothermal ore deposits: Nature, v. 370(6490), p. 519–527.

Hersum, T., Hilpert, M., and Marsh, B., 2005, Permeability and melt flow in simulated and natural partially molten basaltic magmas: Earth and Planetary Science Letters, v. 237, p. 798–814.

Horita, J., and Wesolowski, D.J., 1994, Liquid-vapor fractionation of oxygen and hydrogen isotopes of water from the freezing to the critical temperature: Geochimica et Cosmochimica Acta, v. 58, p. 3425–3437.

Hou, T., Charlier, B., Holtz, F., Veksler, I., Zhang, Z., Thomas, R., and Namur, O., 2018, Immiscible hydrous Fe-Ca-P melt and the origin of iron oxide-apatite ore deposits: Nature Communications 9(1) no. 1415.

Huang, F., Zhang, Z., Lundstrom, C.C., and Zhi, X., 2011, Iron and magnesium isotopic compositions of peridotite xenoliths from eastern China: Geochimica et Cosmochimica Acta, v. 75, p. 3318–3334.

Knipping, J.L., Bilenker, L.D., Simon, A.C., Reich, M., Barra, F., Deditius, A.P., Lundstrom, C., Bindeman, I., and Munizaga, R., 2015a, Giant Kiruna-type deposits form by efficient flotation of magmatic magnetite suspensions: Geology, v. 43, p. 491–594.

Knipping, J.L., Bilenker, L.D., Simon, A.C., Reich, M., Barra, F., Deditius, A.P., Wälle, M., Heinrich, C.A., Holtz, F., and Munizaga, R., 2015b, Trace elements in magnetite from massive iron oxide-apatite deposits indicate a combined formation by igneous and magmatic hydrothermal processes: Geochimica et Cosmochimica Acta, v. 171, p. 15–38.

Knipping, J., Fiege, A., Simon, A.C., Oeser, M., Reich, M., and Bilenker, L., 2019a, In-situ iron isotope analyses reveal igneous and magmatic-hydrothermal growth of magnetite at the Los Colorados Kiruna-type iron oxide-apatite deposit, Chile: American Mineralogist, v. 104, p. 471–484.

Knipping, J., Webster, J.D., Simon, A.C., and Holtz, F., 2019b, Accumulation of magnetite by flotation on bubbles during decompression of silicate magma: Scientific Reports, v. 9, p. 3852.

Kyser, T.K., Lesher, C.E., and Walker, D., 1998, The effects of liquid immiscibility and thermal diffusion on oxygen isotopes in silicate liquids: Contributions to Mineralogy and Petrology, v. 133, p. 373–381.

La Cruz, N.L., Ovalle, J.T., Simon, A.C., Konecke, B.A., Barra, F., Reich, M., Leisen, M., and Childress, T.M., 2020, The geochemistry of magnetite and apatite from the El Laco iron oxide-apatite deposit, Chile: Implications for ore genesis: Economic Geology, v. 115, p. 1461-1491

Le Maitre, R.W., Streckeisen, A., Zanettin, B., Le Bas, M.J., Bonin, B., and Bateman, P., eds., 2005, Igneous rocks: A classification and glossary of terms: Recommendations of the International Union of Geological Sciences Subcommission on the Systematics of Igneous Rocks: U.K., Cambridge University Press, 236 p.

Lester, G.W., Clark, A.H., Kyser, T.K., and Naslund, H.R., 2013a, Experiments on liquid immiscibility in silicate melts with $H_2O$, P, S, F and Cl: Implications for natural magmas: Contributions to Mineralogy and Petrology, v. 166 p. 329–349.

Lester, G.W., Kyser, T.K.., and Clark, A.H., 2013b, Oxygen isotope partitioning between immiscible silicate melts with $H_2O$, P and S: Geochimica et Cosmochimica Acta, v. 109, p. 306–311.

Lindsley, D.H., 1962, Investigations in the system $FeO$-$Fe_2O_3$-$TiO_2$: Carnegie Institution of Washington Yearbook, v. 61, p. 100–106.

——1963, Equilibrium relations of coexisting pairs of Fe-Ti oxides: Carnegie Institution of Washington Year Book, v. 62, p. 60–66.

——1991, Experimental studies of oxide minerals: Reviews in Mineralogy, v. 25, p. 69–106.

Loewen, M.W., and Bindeman, I.N., 2016, Oxygen isotope thermometry reveals high magmatic temperatures and short residence times in Yellowstone and other hot-dry rhyolites compared to cold-wet systems: American Mineralogist, v. 101(5), p. 1222–1227.

Maksaev, V., Gardeweg, M., Ramírez, C.F., and Zentilli, M., 1988, Aplicación del método trazas de fisión a la datación de cuerpos de magnetita de El Laco e Incahuasi en el Altiplano de la Región de Antofagasta: V Congreso Geológico Chileno, Actas, 1:B1–B23.

Matthews, A., Goldsmith, J.R., and Clayton, R.N., 1983, Oxygen isotope fractionation involving pyroxenes: The calibration of mineral-pair geothermometers: Geochimica et Cosmochimica Acta, v. 47, p. 631–644.

Matthews, S.J., Sparks, R.S.J., and Gardeweg, M.C., 1999, The Piedras Grandes–Soncor eruptions, Lascar volcano, Chile; evolution of a zoned magma chamber in the central Andean upper crust: Journal of Petrology, v. 40(12), P. 1891–1919.

Miller, M.F., Pack, A., Bindeman, I.N., and Greenwood, R.C., 2020, Standardizing the reporting of $\Delta^{17}O$ data from high precision oxygen triple-isotope ratio measurements of silicate rocks and minerals: Chemical Geology, v. 532, p. 119332.

Millet, M.A., Baker, J.A., and Payne, C.E., 2012, Ultra-precise stable Fe isotope measurements by high resolution multiple-collector inductively coupled plasma mass spectrometry with a $^{57}Fe$-$^{58}Fe$ double spike: Chemical Geology, v. 304, p. 18–25.

Moore, G., and Carmichael, I., 1998, The hydrous phase equilibria (to 3 kbar) of an andesite and basaltic andesite from western Mexico: Constraints on water content and conditions of phenocryst growth: Contributions to Mineralogy and Petrology, v. 130, p. 304-319, doi:10.1007/s004100050367.

Müller, J., 1995, Oxygen isotopes in iron (II) oxides: A new preparation line: mineral-water fractionation factors and paleoenvironmental considerations: Isotopes in Environmental and Health Studies, v. 31, p. 301–302.

Naranjo, J.A., Henríquez, F., and Nyström, J.O., 2010, Subvolcanic contact metasomatism at El Laco Volcanic Complex, Central Andes: Andean Geology, v. 37, p. 110–120.

Naslund, H.R., 1983, The effect of oxygen fugacity on liquid immiscibility in iron-bearing silicate melts: American Journal of Science, v. 283, p. 1034–1058.

Naslund, H.R., Henriquez, F., Nyström, J.O., Vivallo, W., and Dobbs, F.M., 2002, Magmatic iron ores and associated mineralisation: Examples from the Chilean high Andes and coastal Cordillera, *in* Porter, T.M., ed., Hydrothermal iron oxide copper–gold: A global perspective, 2: Adelaide, Australia, PGC Publishing, p. 207–226.

Naslund, H.R., Mungall, J.E., Henriquez, F., Nyström, J.O., Lledó, H., Lester, G.W., and Aguirre, R., 2009, Melt inclusions in silicate lavas and iron-oxide tephra of the El Laco volcano: Congreso Geológico Chileno, XII, Santiago, Chile, Proceedings, p. 23–26.

Nyström, J.O., Billström, K., Henríquez, F., Fallick, A.E., and Naslund, H.R., 2008, Oxygen isotope composition of magnetite in iron ores of the Kiruna type in Chile and Sweden: GFF [Geologiska Föreningen], v. 130, p. 177–188.

Nyström, J.O., Henríquez, F., Naranjo, J.A., and Nasuland, H.R., 2016, Magnetite spherules in pyroclastic iron ore at El Laco, Chile: American Mineralogist, v. 101, p. 587–595.

Ovalle, J.T., La Cruz, N.L., Reich, M., Barra, F., Simon, A.C., Konecke, B.A., Rodriguez-Mustafa, M.A., Deditius, A.P., Childress, T.M., and Morata, D., 2018, Formation of massive iron deposits linked to explosive volcanic eruptions: Nature Scientific Reports, v. 8, no. 14855.

Pack, A., Tanaka, R., Hering, M., Sengupta, S., Peters, S., and Nakamura, E., 2016, The oxygen isotope composition of San Carlos olivine on the VSMOW2-SLAP2 scale: Rapid Communications in Mass Spectrometry, v. 30, p. 1495–1504.

Park, C.F., Jr., 1961, A magnetite "flow" in northern Chile: Economic Geology, v. 56, p. 431–436.

Philpotts, A.R., 1967, Origin of certain iron-titanium oxide and apatite rocks: Economic Geology, v. 62, p. 303–315.

Pleše, P., Higgins, M.D., Mancini, L., Lanzafame, G., Brun, F., Fife, J.L., Casselman, J., and Baker, D.R., 2018, Dynamic observations of vesiculation reveal the role of silicate crystals in bubble nucleation and growth in andesitic magmas: Lithos, v. 296–299, p. 532–546.

Qi, H., Coplen, T.B., Gehre, M., Vennemann, T.W., Brandt, W.A., Geilmann, H., Olack, G., Bindeman, I.N., Palandri, J., Huang, L., and Longstaffe, F.J., 2017, New biotite and muscovite isotopic reference materials, USGS57 and USGS58, for $\delta^2H$ measurements—a replacement for NBS 30: Chemical Geology, doi:10.1016/j.chemgeo.2017.07.027.

Rhodes, A.L., and Oreskes, N., 1995, Magnetite deposition at El Laco, Chile: Implications for Fe-oxide formation in magmatic-hydrothermal systems: Giant Ore Deposits Workshop, 2nd, April 25-27, 1995, Queens University, Kingston, Ontario, Canada, Proceedings, p. 582–622.

——1999, Oxygen isotope composition of magnetite deposits at El Laco, Chile: Society of Economic Geologists Special Publication 7, p. 333–351.

Rhodes, A.L., Oreskes, N., and Sheets, S., 1997, Recognition of a paleohydrothermal system responsible for magnetite formation at El Laco, Chile: Transactions of the American Geophysical Union, EOS Supplement 46, p. 748–749.

——1999, Geology and rare earth element (REE) geochemistry of magnetite deposits at El Laco, Chile: Society of Economic Geologists Special Publication 7, p. 299–332.

Sheets, S.A., Oreskes, N., Rhodes, A.L., Bodnar, R.J., and Szabo, C., 1997, Fluid inclusion evidence for a hydrothermal origin for magnetite-apatite mineralization at El Laco, Chile: Geological Society of America Abstracts with Programs, 2:A50.

Sillitoe, R.H., and Burrows, D.R., 2002, New field evidence bearing on the origin of the El Laco magnetite deposit, northern Chile: Economic Geology, v. 97, p. 1101–1109.

Simon, A.C., Pettke, T., Candela, P.A., Piccoli, P.M., and Heinrich, C.A., 2004, Magnetite solubility and iron transport in magmatic-hydrothermal environments: Geochimica et Cosmochimica Acta, v. 68(23), p. 4905–4914.

Simon, A.C., Knipping, J., Reich, M., Barra, F., Deditius, A.P., Bilenker, L., and Childress, T., 2018, Kiruna-type iron oxide-apatite (IOA) and iron oxide copper-gold (IOCG) deposits form by a combination of igneous and magmatic-hydrothermal processes: Evidence from the Chilean iron belt: Society of Economic Geology Special Publication no. 21, p. 89–114.

Taylor, B.E., Eichelberger, J.C., and Westrich, H.R., 1983, Hydrogen isotopic evidence of rhyolitic magma degassing during shallow intrusions and eruption: Nature, v. 306, p. 541–545.

Taylor, H.P., Jr., 1967, Oxygen isotope studies of hydrothermal mineral deposits, *in* Barnes, H.L., ed., Geochemistry of hydrothermal ore deposits, 1st ed.: New York, Holt, Rinehart and Winston, p. 109–142.

——1968, The oxygen isotope geochemistry of igneous rocks: Contributions to Mineralogy and Petrology, v. 19, p. 1–71.

——1974, The application of oxygen and hydrogen isotope studies to problems of hydrothermal alteration and ore deposition: Economic Geology, v. 69, p. 843–883.

Taylor, H.P., Jr., and Epstein, S., 1966, Deuterium-hydrogen ratios in coexisting minerals of metamorphic and igneous rocks [abs.]: American Geophysical Union Transactions, v. 47, p. 213.

Tornos, F., Velasco, F., and Hanchar, J.M., 2016, Iron-rich melts, magmatic magnetite, and superheated hydrothermal systems: The El Laco deposit, Chile: Geology, v. 44, p. 427–430.

——2017, The magmatic to magmatic-hydrothermal evolution of the El Laco deposit (Chile) and its implications for the genesis of magnetite-apatite deposits: Economic Geology v. 112, p. 1595–1628.

Troll, V.R., Weis, F.A., Jonsson, E., Andersson, U.B., Majidi, S.A., Hogdahl, K., Harris, C., Millet, M-A., Saravanan, C., Kooijman, E., and Nilsson, K.P., 2019, Global Fe-O isotope correlation reveals magmatic origin of Kiruna-type apatite-iron-oxide ores: Nature Communications, v. 10, p. 1712 PMCID: PMC6461606.

Tucker, P., and O'Reilly, W., 1980, The laboratory simulation of deuteric oxidation of titanomagnetites: Effect on magnetic properties and stability of thermoremanence: Physics of the Earth and Planetary Interiors, v. 23(2), p. 112–133.

Velasco, F., Tornos, F., and Hanchar, J.M., 2016, Immiscible iron-and silica-rich melts and magnetite geochemistry at the El Laco volcano (northern Chile): Evidence for a magmatic origin for the magnetite deposits. Ore Geology Reviews v. 79, p. 346–366.

Vivallo, W., Henríquez, F., and Espinoza, S., 1994, Oxygen and sulfur isotopes in hydrothermally altered rocks and gypsum deposits at El Laco mining

district, northern Chile: Departamento de Geología, Universidad de Chile, Comunicaciones, v. 45, p. 93–100.
Waterisotopes Database, 2018, http://waterisotopes.org, Accessed 11/20/2018.
Webster, J.D., 1997, Exsolution of magmatic volatile phases from Cl-enriched mineralizating granitic magmas and implications for ore metal transport: Geochimica et Cosmochimica Acta, v. 61, p. 1017–1029.
Weis, F., 2013, Oxygen and iron isotope systematics of the Grängesberg mining district (GMD), central Sweden: Ph.D. Dissertation, Uppsala, Sweden, Uppsala Universitet, 77 p.
Xie, Q., Zhang, Z., Hou, T., Cheng, Z., Campos, E., Wang, Z., and Fei, X., 2019, New insights for the formation of Kiruna-type iron deposits by immiscible hydrous Fe-P melt and high-temperature hydrothermal processes: Evidence from El Laco deposit: Economic Geology, v. 114, p. 35–46.
Yapp, C.J., and Pedley, M.D., 1985, Stable hydrogen isotopes in iron oxides. II. D/H variations among natural goethites: Geochimica et Cosmochimica Acta, v. 49, p. 487–495.
Zajacz, Z., Halter, W.E., Pettke, T., and Guillong, M., 2008, Determination of fluid/melt partition coefficients by LA-ICPMS analysis of co-existing fluid and silicate melt inclusions: controls on element partitioning. Geochimica et Cosmochimica Acta, v. 72(8), p. 2169–2197.
Zakharov, D.O., and Bindeman, I.N., 2019, Triple oxygen and hydrogen isotopic study of hydrothermally altered rocks from the 2.43-2.41 Ga Vetreny belt, Russia: An insight into the early Paleoproterozoic seawater: Geochimica et Cosmochimica Acta, v. 248, p. 185–209, doi: 10.1016/j.gca.2019.01.014.
Zakharov, D.O., Bindeman, I.N., Slabunov, A.I., Ovtcharova, M., Coble, M.A., Serebryakov, N.S., and Schaltegger, U., 2017, Dating the Paleoproterozoic snowball Earth glaciations using contemporaneous subglacial hydrothermal systems: Geology, v. 45, p. 667–670, doi:10.1130/G38759.1.
Zhao, Z-F., and Zheng, Y-F, 2003, Calculation of oxygen isotope fractionation in magmatic rocks: Chemical Geology, v. 193, p. 59–80.

**Tristan Childress** is currently an exploration geologist for Wellborn Mining, LLC, at the historical Hog Mountain orogenic gold deposit located in the southern Piedmont of Alabama, USA. He received his B.S. degree in geology from the University of South Carolina in 2012 and his Ph.D. from the University of Michigan in 2019. Utilizing stable isotopes and minor and trace elements in iron oxides to compare iron oxide-apatite (IOA) and iron oxide copper-gold (IOCG) deposits was the focus of his doctoral thesis. Tristan's experience ranges from the IOA and IOCG deposits of Chile to exploration at the Red Dog Pb-Zn deposit in Alaska and his present work in the orogenic gold of Alabama.